INSTITUTO
UNIVERSITÁRIO
DE LISBOA

Short-Reach 200 Gb/s SDM network employing direct-detection and optical SSBI mitigation

Tiago David Freitas Marques

Master in Telecommunications and Computer Engineering

Supervisor:
Doctor Tiago Manuel Ferreira Alves, Assistant Professor,
ISCTE - Instituto Universitário de Lisboa

Co-Supervisor:
Doctor Adolfo da Visitação Tregeira Cartaxo, Full Professor,
ISCTE - Instituto Universitário de Lisboa

December, 2020

This is for my mom and dad. Forever grateful for all your love and support.

Acknowledgments

First of all, I would like to express my deepest gratitude to Professor Tiago Alves and Professor Adolfo Cartaxo for all their availability, encouragement and guidance throughout this process. Their patience and willingness to help me day after day were fundamental to complete this dissertation.

I would also like to thank my family for their unconditional love and for all their efforts to make this possible.

I would like to acknowledge my closest friends for all their friendship and support, contributing in a fundamental way to achieve my goals.

Lastly, I want to express my heartiest appreciation for my girlfriend, Catarina Pestana, for having been my cornerstone from the beginning to the end of this journey. Thank you for always being by my side, for never letting me give up, and, above all, for your genuine friendship.

Resumo

De modo a responder às crescentes exigências de capacidade das redes óticas de próxima geração, nesta dissertação propõe-se um esquema inovador de transmissão para redes de curto alcance baseado em deteção-direta (DD) e fibras multinúcleo (MCF), com um núcleo dedicado à transmissão de portadoras e os restantes núcleos dedicados à transmissão dos sinais. Com este esquema, pode ser implementada uma abordagem de mitigação da interferência do batimento sinal-sinal (SSBI) de baixa complexidade. Isto pode ser de particular interesse para sistemas que requerem compensação eletrónica da dispersão cromática (CD) no lado do recetor. O desempenho de um sinal NRZ polar de 200 Gb/s numa rede MCF de curto alcance utilizando o esquema de transmissão proposto limitado pela CD e pelo efeito combinado do atraso relativo de propagação (skew) e do ruído de fase do laser é avaliado através de simulação numérica.

Os resultados mostram que os sistemas que utilizam lasers com maiores larguras de linha tornam-se mais vulneráveis ao skew, limitando mais o desempenho do sistema devido à conversão do ruído de fase em intensidade. Quando a CD não é compensada, a utilização da técnica de mitigação da SSBI permite distâncias até 180 m, mostrando potencial para ser implementada dentro de centros de dados. Estes resultados são obtidos quando a potência ótica média do sinal é 18 dB superior à potência ótica média da portadora, e quando a estimação da SSBI não é corrompida pelo ruído elétrico. No entanto, o potencial mais elevado do esquema de transmissão proposto poderá ser alcançado para sistemas em que o efeito da CD é compensado eletronicamente no lado do recetor. Para sistemas com compensação total de CD, os resultados mostram uma melhoria significativa do desempenho obtida pela abordagem de mitigação da SSBI implementada.

Palavras-chave: interferência de batimento sinal-sinal, atraso relativo de propagação, ruído de fase do laser, deteção-direta, fibras multinúcleo, redes de curto alcance.

Abstract

In order to respond to the growing capacity demands of next-generation optical networks, this dissertation proposes an innovative transmission scheme for direct-detection (DD) multi-core fibre (MCF) short-reach networks with one core dedicated to carriers transmission and the remaining cores dedicated to signals transmission. With this scheme, a low-complexity signal-signal beat interference (SSBI) mitigation approach can be employed. This may be of particular interest for systems requiring electronic chromatic dispersion (CD) compensation at the receiver side. The performance of a 200 Gb/s polar non-return-to-zero (NRZ) signal in a MCF short-reach network employing the proposed transmission scheme impaired by CD and the combined effect of the skew and the laser phase noise is evaluated through numerical simulation.

The results show that systems employing lasers with broader linewidths become more sensitive to the skew, limiting further the system performance due to phase-to-intensity conversion. When CD is not compensated, employing the SSBI mitigation technique enables distances up to 180 m, showing potential to be implemented in intra data centre networks. These results are obtained when the signal mean optical power is 18 dB higher than the carrier mean optical power, and when the SSBI estimation is not corrupted by electrical noise. Nevertheless, the higher potential of the proposed transmission scheme may be achieved for systems in which the CD effect is compensated electronically at the receiver side. For systems with full CD compensation, the results show a significant performance improvement obtained by the SSBI mitigation approach employed.

Keywords: signal-signal beat interference, skew, laser phase noise, direct-detection, multi-core fibre, short-reach networks.

Contents

List of Figures

List of Tables

List of Acronyms

APD	**A**valanche **P**hotodiode
BER	**B**it **E**rror **R**ate
CAPEX	**C**apital **E**xpenditure
CD	**C**hromatic **D**ispersion
CW	**C**ontinuous **W**ave
DC	**D**ata **C**entre
DCF	**D**ispersion **C**ompensation **F**ibre
DD	**D**irect-**D**etection
DEC	**D**irect-**E**rror **C**ounting
DFB	**D**istributed **F**eed**b**ack Laser
DSP	**D**igital **S**ignal **P**rocessing
ECL	**E**xternal **C**avity **L**aser
EDFA	**E**rbium-**D**oped **F**ibre **A**mplifier
EOP	**E**ye-**O**pening **P**enalty
FBG	**F**ibre **B**ragg **G**ratings
FEC	**F**orward **E**rror **C**orrection
FMF	**F**ew-**M**ode **F**ibre
ICXT	**I**ntercore **C**rosstalk
IM-DD	**I**ntensity **M**odulation **D**irect-**D**etection
ISP	**I**nternet **S**ervice **P**rovider
KK	**K**ramers-**K**ronig
LED	**L**ight **E**mitting **D**iode
MBP	**M**inimum **B**ias **P**oint
MCF	**M**ulti-**C**ore **F**ibre
MIMO	**M**ultiple-**I**nput **M**ultiple-**O**utput

MMF	**M**ulti-**M**ode **F**ibre
MZM	**M**ach **Z**ehnder **M**odulator
NRZ	**N**on-**R**eturn-to-**Z**ero
OCT	**O**uter **C**ladding **T**hickness
OPEX	**O**perational **E**xpenditure
PAM	**P**ulse **A**mplitude **M**odulation
PD	**P**hotodiode
PDI	**P**ropagation-**D**irection **I**nterleaving
PDM	**P**olarization-**D**ivision **M**ultiplexing
PIN	**P**ositive-**I**ntrinsic-**N**egative
PMD	**P**olarization **M**ode **D**ispersion
PSD	**P**ower **S**pectral **D**ensity
QAM	**Q**uadrature **A**mplitude **M**odulation
QBP	**Q**uadrature **B**ias **P**oint
SCF	**S**ingle **C**ore **F**ibre
SDM	**S**pace-**D**ivision **M**ultiplexing
SE	**S**pectral **E**fficiency
SM-MCF	**S**ingle-**M**ode **M**ulti-**C**ore **F**ibre
SM-SCF	**S**ingle-**M**ode **S**ingle-**C**ore **F**ibre
SNR	**S**ignal-to-**N**oise **R**atio
SSBI	**S**ignal-**S**ignal **B**eat **I**nterference
SSC	**S**uper **S**patial **C**hannel
SSMF	**S**tandard **S**ingle-**M**ode **F**ibre
WDM	**W**avelength-**D**ivision **M**ultiplexing
XT	**C**rosstalk

List of Symbols

A_c	Amplitude of the optical carrier
$B_{-3\,dB}$	-3 dB bandwidth of the electrical filter
$B_{e,n}$	Noise equivalent bandwidth of the electrical filter
B_n	n-th order Bessel polynomial
c	Speed of light in vacuum
D_λ	Dispersion parameter
$e_{out(t)}$	Electrical field at the output of the MZM
$\|e_{PIN}(t)\|^2$	Instantaneous power of the optical signal at the input of the PIN
E_c	Electrical field of the carrier
E_{in}	Electrical field at the input of the MZM
E_{sig}	Electrical field of the NRZ signal
$f_{n,e}$	Noise figure
f_s	Sampling frequency
h	Planck constant
$h(t)$	Impulse response of the SM fibre
$H(f)$	Bessel filter transfer function
$H_f(\omega)$	SSMF transfer function
$i_A(t)$	Photocurrent at the output of PIN A
$i_B(t)$	Photocurrent at the output of PIN B
i_l	Insertion loss of the MZM
I_1	Lowest current associated with bits 1
I_0	Highest current associated with bits 0
I_{av}	Average current
$n_e(t)$	Electrical noise
k_B	Boltzmann constant

L	Fibre length
P_c	Carrier mean optical power
P_{noise}	Noise power
P_r	Relative power level
P_s	NRZ signal mean optical power
P_{tot}	Carrier-added NRZ signal mean power at the output of PIN A
q	Electron charge
R_λ	PIN responsivity
$s_{in}(t)$	Data signal at the MCF input
S_{λ_0}	Dispersion slope parameter at the wavelength λ_0
t_c	Laser phase noise coherence time
T_s	Skew
T_W	Simulation time window
v_{ac}	Data signal at the input of the MZM
V_b	Bias voltage of the MZM
V_{sv}	Switching voltage of the MZM
α	Fibre loss coefficient
$\Delta\nu_L$	Laser linewidth
η	Photodetection efficiency
ν	Optical frequency of the incident optical signal
ω	Angular frequency
β_0	Phase velocity
β_1	Propagation time delay
v_g	Group velocity
λ_0	Operating optical wavelength
$\phi_n(t)$	Phase noise of the optical source
σ_c^2	Power of the circuit noise

Chapter 1

Introduction

This dissertation assesses the performance of a short-reach multi-core fibre (MCF) based space-division multiplexing (SDM) network employing direct-detection (DD) receivers. These receivers cause performance degradation induced by signal-signal beat interference (SSBI) and so this work proposes an innovative transmission scheme, which enables a low-complexity SSBI mitigation technique. The effects of the main operational issues related to DD-based MCF systems are evaluated in order to specify the possible application scenarios for the proposed transmission scheme.

1.1 Motivation

In the context of optical fibre networks there is an exponential growth on the demands of their capacity due to the increased internet data traffic caused by the continuous rise of connected devices, cloud services and other online services [1], forcing the communication networks to adopt strategies as advanced modulation and multiplexing schemes, like wavelength-division multiplexing (WDM), advanced forward error correction (FEC) codes that allow a bit error rate of 10^{-3} before applying the codes and low-loss fibre to allow better spectral efficiencies (SE) [3]. Nevertheless, with long-term traffic growing at a rate of approximately 60% per year [4], it leads to a scenario where these networks will not be able to keep up with the requirements necessary for their acceptable functioning. To avoid this so-called capacity crunch (around 100 Tb/s), space-division multiplexing has been pointed out and intensively studied to become the solution for this problem

[5].

Due to the limitations of bandwidth scaling and limited amplifier bandwidth of single-mode single-core fibre (SM-SCF) systems, space is the remaining option to boost network's capacities; this will come with the integration of SDM with implemented WDM systems (WDM x SDM). SDM is a powerful alternative to provide an ultimate capacity increase as it explores the only physical dimension left to be exploited in optical networks. This becomes particularly appealing to data centre (DC) traffic, where the need to scale the increasing throughput is of primary importance. To do so, WDM solutions show great potential as it allows to transmit multiple signals at different wavelengths in one single-core fibre. By incorporating this technology with SDM, the capacity of the network will ideally increase in proportion to the number of cores used.

As for short-reach connections, like intra DC communications, it has been experiencing data traffic growth due to the online services they provide, leading to the appearance of more data centres and hyperscale data centres [1]. This phenomenon will bring constrains such as the space limitations in short-reach networks and the need to maximize the throughput of each connection.

In order to avoid the stagnation of today's networks, new techniques to improve system capacity are needed. In this work, an innovative MCF intensity-modulated direct-detection (IM-DD) optical system is proposed. However, DD receivers cause performance degradation induced by SSBI which can corrupt the data signal delivered to the receiver. This effect is highly emphasised depending on the laser linewidth used and the skew between the homogeneous cores of the MCF, so it is important to analyse to what extend the system can accommodate their impact. This work will examine a new approach based on signal-signal beat interference mitigation without complex digital signal processing (DSP) to increase the network's capacity while maintaining a low-complexity and a low-cost architecture, that can enable a cost-effective evolution for short-reach networks that are growing rapidly and demand immediate solutions. Also, with the proposed transmission scheme, in which the carriers are transmitted independently from the data signals, additional cost savings may be achieved in bidirectional networks. This occurs because local lasers can be replaced by a single optical comb with carriers being distributed as optical seeds in a single MCF core along the whole network.

1.2 Research questions

This work aims to respond the following main questions:

- How can MFC-based SDM respond to the growing capacity demands on networks?
- How can MCF help manage the space limitations in intra data centre communications?
- How can performance degradation induced by SSBI in DD systems be overcome?
- With the proposed network approach, which is the maximum reach allowed for the data centre?

1.3 Objectives

The main goal of this dissertation is to enable the capacity growth and provide a significant increase of users supported by next-generation optical access networks. This is done by elaborating a SDM short-reach network with a dedicated capacity per user of 200 Gb/s, using direct-detection receivers and a new technique for SSBI mitigation. The main objectives of this work are:

- To integrate a software platform for simulation of short-reach 200 Gb/s SDM optical fibre networks employing DD and optical SSBI mitigation;
- To identify the main operational obstacles of the proposed SDM network;
- To specify the maximum skew of homogeneous MCF, the laser linewidth and the maximum reach for short-reach networks employing the proposed SSBI mitigation technique.

1.4 Structure of the dissertation

This dissertation has the following structure, split into five chapters and two appendixes. In chapter 2, the fundamental concepts related to data centres, MCFs and DD receivers

are described. The SSBI issue is introduced and reviewed in detail. In chapter 3, the description of the proposed IM-DD system to mitigate the SSBI is presented and the effects of the main performance impairments on the 200 Gb/s non-return-to-zero (NRZ) polar signal are assessed, namely the combined effect of the skew and the laser phase noise. In chapter 4, the impact of the skew, the laser phase noise and chromatic dispersion on the system performance are quantified through bit error rate (BER) measurements. The results are analysed and the validity of the proposed SSBI mitigation technique is discussed. In chapter 5, the final conclusions of this work are presented. In Appendix A, it can be found the description of the electrical noise model used in some of the simulations. Finally, Appendix B describes the BER method utilised to evaluate the performance of the IM-DD system.

1.5 Original contributions

In the author's opinion, the main original contributions of this dissertation are:

- Proposal of an innovative MCF transmission scheme with one core dedicated to transmit the virtual carriers used to assist the detection and the remaining cores dedicated to transmit the data signals;
- Proposal of a low-complexity SSBI mitigation technique;
- Evaluation of the performance of 200 Gb/s MCF short-reach network employing DD considering the combined effect of skew, laser phase noise and chromatic dispersion;
- Identification of the maximum skew supported by different laser linewidths and the maximum reach when employing the proposed SSBI mitigation technique.

Chapter 2

Fundamental concepts

In this chapter, the fundamental concepts associated to short-reach DD-based MCF optical systems are presented. Firstly, in sections 2.1, 2.2 and 2.3, the state-of-the art related to data centres, space-division multiplexing and multi-core fibres is reviewed, respectively. In subsection 2.3.1, the crosstalk in weakly-coupled MCFs is discussed. Finally, in section 2.4, the optical receiver based on direct-detection is described and the SSBI problematic is detailed.

2.1 Data centre interconnections

Nowadays, with the changes that traffic patterns are suffering, DCs are fundamental for delivering IT services and providing storage, communications and networking to the growing number of connected devices and users [1]. Until now, DC networks were mainly based on electronic packet switches but this comes in a price of not being cost-effective to accommodate the increased communication bandwidth needed, thus starting to arise the need for other solutions, such as optical interconnects [6], [7]. These optical interconnects offer the high bandwidth and density that are fundamental for DCs to oppose bottlenecks in the infrastructure elements (e.g., switch and front panel) [8]. As DC traffic requirements increases to values of Tbps, adopting all-optical interconnects (similarly to current telecommunication networks) could be the solution to keep up with the high traffic needs whilst decreasing power consumption [9]. According to [10], adopting all-optical networks could provide up to 75% energy savings in DCs; in the

particular case for large DC (hyperscale DC) where high bandwidth, power efficiency and low latency is needed, the implementation of optical interconnects is crucial and is seen with major interest [11].

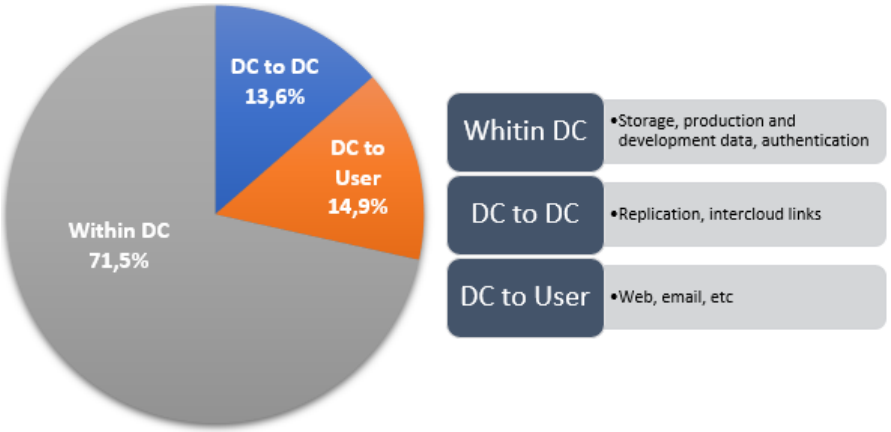

Figure 2.1: DC traffic destination by 2021 [1].

As it can be observed in Figure 2.1, it is estimated that by 2021 85% of the traffic will correspond to east-west flow, that is, DC-to-DC and within DC traffic. The evolved characteristics of applications hosted in the DC (like cloud computing and search engines) demand high interactivity between servers in the DC [12] which require more efficient interconnections. Actual DC networks present high power consumption and require high number of links to interconnect the different level switches, not being adequate to fulfil the demands for future interconnection schemes [13]. In [6], it is presented several optical interconnect schemes for DC that have been proposed in recent research. These new interconnect schemes need to be designed based on the new way that traffic is forwarded, moving from a north-south pattern (traffic from outside DCs to servers) to an east-west traffic management [14].

On one hand, intra DC interconnects means connections within the data centre and typically reach up to 10 km or less. In this case, nonlinear effects are negligible due to the short size of the links and they operate with relatively small power levels near 1310 nm to minimize total chromatic dispersion (CD). On the other hand, inter DC connections characterize links between data centres, that can reach up to 100 km and operate around 1550 nm to potentiate the use of erbium-doped fibre amplifiers (EDFA). The latter (inter DC connections) needs CD compensation and it can be done by dispersion compensation fibres (DCFs) or tuneable fibre Bragg gratings (FBGs) [14]. These two DC schemes should employ Mach-Zehnder modulators (MZM) due to the negligible

chirp, high bandwidth and the possibility to generate high-order pulse amplitude modulation (PAM) and quadrature amplitude modulation (QAM); this type of MZMs would require extra segments to support phase shaping but can lead to power and complexity savings [14].

In terms of the fibre employed in inter and intra data centre networks, although the propagation impairments as polarization mode dispersion (PMD) and nonlinearities are often negligible regarding these short-reach connections [14], single core fibres (SCF) are not a viable solution because of space limitations and transmission constrains associated with size, cost and power consumption. Therefore, MCF is seen as a good solution to maximize the capacity of the transmission link bandwidth and density of short-reach connections. To facilitate the integration of MCFs for DC applications, this new type of fibre must not show too much discrepancy between standard fibre parameters such as dimensions and optical properties. In [15], the authors proposed different types of MCFs suitable for short-reach applications that are compatible with the standard 250 microns diameter coating.

Conditioned by cost purposes, MCF-based short-reach networks should employ direct-detection receivers, as this kind of receivers features a less complex implementation scheme; however, it can limit the link reach and brings up SSBI problems.

2.2 Space-division multiplexing

Until now, networks employed SM-SCF to transmit data and they achieved a maximum transmission rate of around 100 Tb/s, associated with the Shannon limit for SM-SCF caused by the signal bandwidth and the noised induced by the linear and non-linear effects [16]. This setback is pointed to be solved by the emerging SDM and due to this, there has been an “around the world” research on SDM and its viability [4], [16]. SDM can be broadly described as multiple independent spatial channels for optical data transmission, designed to enhance the network’s capacity in several orders of magnitude, overcoming the nonlinear Shannon limit of conventional fibre [3].

To increase data throughput, networks need to be adjustable and elastic, dynamically adapting itself to unexpected traffic patterns and quickly establishing or taking down connections. SDM increases capacity and switching flexibility but adds new challenges to an already complex network [17]. To make the transition to SDM achievable it

must provide other advantages than capacity increase; this technology needs to show benefits in cost-per-bit and energy efficiency [16], two crucial factors for Internet Service Providers (ISP) on a commercial point of view alongside integration. It is unrealistic to anticipate a new fully-SDM network as it would be very expensive but instead the approach that shall be taken is an "upgrade-path". In this solution, SDM components are added to the current infrastructure [16], sharing system components already in use by other technologies (like WDM), and smoothly upgrading the network over time, starting by replacing worn fibre strands for SDM specific fibres. This integration approach is the only viable way for commercial SDM systems to be successfully implemented, reducing capital expenditure (CAPEX) and operational expenditure (OPEX) and still delivering the same reliability of today's networks [3]. Other features provided by SDM is expected to be wavelength contention management and the spatial super channel (SSC), designed to improve the overall behaviour of the network [17].

As the name implies, SDM explores space, the last available multiplexing dimension left to explore in optical communications. In recent years, fibre bundles and polarization-division multiplexing (PDM) have been evolving to more sophisticated techniques and designs [17] that improve the capacity of a single strand of fibre, demonstrating the advantages of SDM. These new ways of using space more efficiently can be based on MCF architectures and few-mode fibre (FMF) transmission techniques. It is also possible a combination of the two aforementioned with few-mode multi-core fibre (FM-MCF) [17].

Regarding to FMF, this type of fibre is basically a multi-mode fibre (MMF), but with 10 or a smaller number of modes where each mode is used to transmit a data stream. In the FMF, coupling between spatial channels is stronger compared with MCFs, which can be used to reduce the group delay spread between modes, but it also increases the complexity of the receiver as it requires multi-input multi-output (MIMO) and DSP. The applications that can utilize this technology are limited due to the fact that all channels need to be received as a whole to avoid data loss [17].

In the case of MCFs, the capacity of the system can be theoretically increased by N times, as N represents the number of independent cores that are incorporated in the same fibre. This way, systems employing MCFs can overcome the capacity crunch already discussed on this work and the space limitation in DC networks. Also, MCFs may potentiate the sharing of network equipment between multiple cores, providing cost reductions [16]. The physically independent single-mode cores arise problems about how

to organise the different cores in order to maximise the capacity of the link and managing the levels of crosstalk (XT), which is an electromagnetic interference induced by the neighbouring cores on each other, normally running in parallel. It has been discovered and studied, both theoretically and then experimentally, innovative ways to counter these impairments associated with MCF, enabling an exponential growth in the capacity of optical networks (discussed in subsection 2.3.1).

There has been experiments on MCFs, achieving capacities up to 305 Tb/s [18], and in order to increase even more MCF transmission rates it is necessary to increase the aggregate SE, defined as a product of the number of cores (N) and the SE per core. In this matter, a recent single-mode multi-core fibre (SM-MCF) transmission experiment have achieved a maximum capacity per fibre of 1.01 Pb/s [19], well beyond the fundamental limit of SM-SCF, and the maximum capacity-distance product obtained was 1.032 Eb/s/fibre·km [20].

2.3 Multi-core fibre

In MCFs, the number of cores will be influenced by crosstalk and several fibre properties such as: core diameter, cladding diameter, outer cladding thickness (OCT) and core pitch, which is the core-to-core distance. The latter is the main fibre parameter which determines the intercore crosstalk (ICXT) levels, arising the need to conduct research to study new designs for MCFs in order to increase core density while minimizing the ICXT [21].

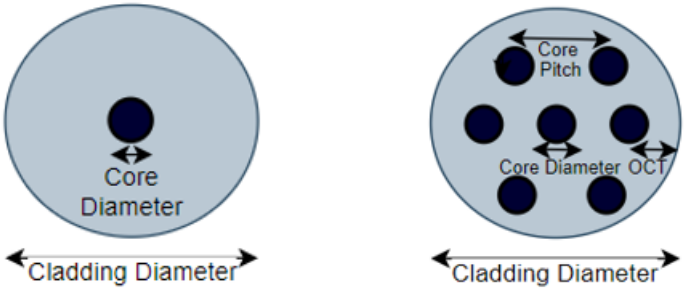

Figure 2.2: Cross section of a single-core fibre and a multi-core fibre.

The fibre coating is constructed with a high refractive index to prevent light leaking from cores into the cladding. For this, outer cores need to have enough OCT (minimum distance between the centre of the outer cores and the fibre borderline) to prevent losses

in the outer cores [20], that can result from bending [20]. In order to easily achieve multiple cores inside the fibre cladding, the cladding diameter tends to grow, as reported by ultra-high-capacity SDM experiments that used thicker fibres with cladding diameters with 200 to 300 microns. Although larger cladding diameters can help reach higher transmission capacities per fibre, it can result in poorer productivity and mechanical reliability of the fibre, as thicker bent fibres have higher breaking probability caused by the higher strain applied to the glass [22].

MCFs can be divided in two main categories concerning the coupling between cores: strongly-coupled and weakly-coupled MCF. Regarding weakly-coupled fibre, it is characterized by core pitches higher than 30 microns, a coupling coefficient lower than 0.01 m^{-1} and each core is used as an individual waveguide with low interference, namely ICXT, between adjacent cores [20]. In weakly-coupled MCFs, complex MIMO DSP is not needed at the receiver to recover the signal [16], as the levels of crosstalk generated are very low. In strongly-coupled MCF, core-to-core distance is deliberately shortened (lower than 30 microns) which results in a more dense core structure with higher levels of crosstalk and the coupling coefficient is bigger than 0.1 m^{-1}, resulting in the need for MIMO DSP to compensate for ICXT.

The MCFs can also be classified as homogeneous, quasi-homogeneous or heterogeneous. In heterogeneous MCFs, each core has a distinct geometry and a slightly different effective refractive index compared with the neighbours. This type of core offers more bend-insensitive and generally lower ICXT. Nevertheless, heterogeneous layouts difficult the fibre design and manufacturing process [17]. In homogeneous MCFs, cores have the same geometry and refractive index and also have the same propagation constant but interchange energy more easily, which provokes increased levels of XT [17]. As for quasi-homogeneous fibres, the cores have minimal variations in the propagation constants originated in the fabrication process, which leads to cores not being perfectly homogeneous. This type of MCFs can also be described as real homogeneous fibres, due to the fact that it is very difficult to achieve the exact same properties for all cores when fabricating homogeneous MCFs.

This work will focus on weakly-coupled homogeneous MCF for short-reach connections (as data centre connections) due to the less complex architecture required compared with other schemes, as heterogeneous MCF and strongly-coupled MCFs.

2.3.1 Intercore crosstalk in weakly-coupled MCFs

When designing an optical network, it is necessary to consider the allowable crosstalk levels that can be supported by the system in order to keep an acceptable function, which can influence the maximum length of the transmission link and the core count within the fibre, consequently affecting the maximum capacity that can be achieved. In the case of MCFs, pointed out as a solution to increase the capacity of optical networks, ICXT represents an impairment that needs to be managed in order to fully exploit the advantages of this uprising transmission technique. In homogeneous MCF-based networks, in which the physical properties of the different cores are nearly identical, the multiple transmitting cores have similar signal propagation times [23] that can originate ICXT due to the coupling between them [24]; this is caused by field interference, external perturbations and physical imperfections along the fibre [17]. The ICXT is a stochastic process and its levels can be influenced by fibre conditions such as fibre bends and twists [25], [26]. The ICXT can significantly affect the quality of the received signal, thus reducing the transmission reach and the overall system performance.

Even though weakly-coupled MCFs are less affected by ICXT than strongly-coupled MCFs, it still can have a high impact on the transmission when high core count and short core pitch distance is used [27], which can lead to high ICXT power levels causing service shutdown or outage over large time periods [28]. This ICXT impacts the signal quality and for this reason, its suppression and characterization has been a primary concern in MCF research in the last few years. In [29], it was experimentally shown the impact of ICXT on a 56-Gbaud PAM4 transmission with a 7-core weakly-coupled MCF, concluding that the ICXT is also dependent on the wavelength, showing that longer wavelengths are more affected by ICXT. In [30], [26] it was also shown that the ICXT is considerably dependent on MCFs parameters, the data modulation format, data-rate and type of optical receiver. Particularly, short-reach networks that employ DD MCF systems using carrier supported signals can be more affected by the dynamic behaviour of ICXT power that may fluctuate significantly over time [30].

Subsequently, there is the need to suppress ICXT effects and it can be done by adopting some crosstalk suppression techniques. One way of doing this is by using trench-assisted MCFs and hole-assisted MCFs that reduces the coupling coefficient between cores, incorporating a low-index trench later around the core [20]. Other approach to suppress crosstalk is to use propagation-direction interleaving (PDI), where

neighbouring cores are assigned in opposite transmission directions to limit the number of adjacent cores that propagates the signal in the same direction, reducing the effective crosstalk between cores [20]. Finally, a third way for reducing crosstalk is by utilizing heterogeneous MCF, as the cores feature different propagation constants, reducing coupling between them.

Still, in the case of short-reach networks, crosstalk is less harmful to the system (comparing with long-haul systems) because accumulated crosstalk is lower, therefore weakly-coupled homogeneous MCF is identified as a solution for data centre applications [15].

2.4 Direct-detection

Regarding the detection process of the signal at the receiver, it can be done either by a coherent detection scheme or by DD. The first one involves the usage of a local oscillator and sophisticated DSPs at receiver site improving the sensitivity, which leads to lower optical power required at the transmitter. However, these receivers have a complex implementation, and even though they can enhance performance and SE, they also increase cost and power consumption [31]. In relation to DD, it has a simple implementation that is optimized to short-reach and point-to-point connections, characterized by being cheaper, smaller and less power hungry than coherent detection systems, hence being suitable for DC connections [32].

In concern to DD, IM-DD is the simplest transmission technique, making it the most cost-effective approach. PAM4 modulation is seen as a good modulation format for optical interconnect and metro networks, derived from its simplicity and ease for signal generation and processing [33]. The IEEE P802.3bs 400GbE Task Force has adopted PAM4 as an industrial standard for DC applications [34]. Other modulation format that can be used in IM-DD systems is the NRZ format, which is the simplest and less complex format available. In [35], it was obtained data rates of 200 Gb/s with PAM4 signals using IM-DD transmission technique, however it only reached distances up to 10km in the O-band, concluding that it was a connection viable for intra data centre but not for data centre interconnecting. In another work [36], it was demonstrated a 182 Gb/s single side band DD transmission using a single photodiode (PD) over 125 km of standard single-mode fibre (SSMF). In [37], it is reported a single polarization and dual-polarization 84

Gbaud PAM4 DD transceiver delivering 168 and 336 Gb/s at 2 and 4 bits per symbol, respectively. In [34], it was demonstrated a real-time end-to-end 53 Gb/s IM-DD-based PAM4 system in the 1550 nm band. This study concluded that PAM4 is a valid alternative for low-cost and high-rate DC interconnections. In [38], it was obtained a transmission of PDM PAM4 signals at the rate of 224 Gb/s and a distance of 10 km using a single IM laser and DD MIMO DSP-based receiver, showing great interest of use for intra DC connections bearing in mind the link reach.

Attending the characteristics of the two detection schemes described above, DD receivers are the most viable option for short-reach networks since it meets the most required requisites of DCs such as lower power consumption and lower cost-per-bit [39]. Still, these receivers cause performance degradation induced by SSBI, and therefore a low-cost and low-complexity solution is sought in order to mitigate this impairment in DD schemes enabling higher data rates and longer connection distances.

2.4.1 Signal-signal beat interference

When DD systems are employed, one of the main problems is related to SSBI and how it can be mitigated. The SSBI component is originated when a signal is detected by a single PD, due to square-law detection [2].

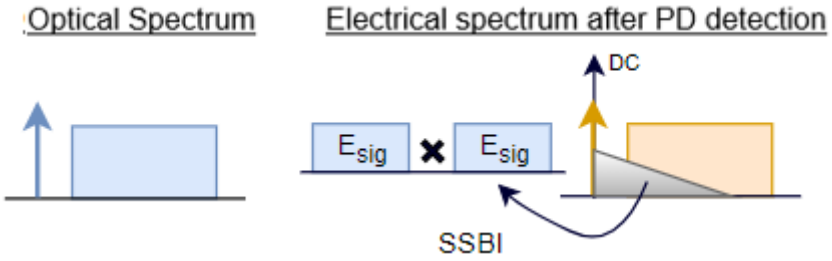

Figure 2.3: SSBI origination [2].

In Figure 2.3 it is shown how the SSBI component is created once the signal is processed by the photodiode; the detected electrical signal can be written as:

$$I_{PD} = |E_c + E_{sig}|^2 = |E_c|^2 + 2 \cdot Re \cdot [E_c^* \cdot E_{sig}] + |E_{sig}|^2 \tag{2.1}$$

where E_{sig} and E_c represent the signal and the carrier, respectively. The last term of equation 2.1 represents the unwanted SSBI component, that falls into the signal band, degrading its quality [2].

If SSBI is removed, the signal can be perfectly detected at the receiver and for this reason, SSBI has been an active research area over the last years. In terms of techniques already studied so far for this matter, the most promising SSBI cancellation techniques include Kramers-Kronig (KK) field reconstruction and iterative SSBI cancellation schemes. For KK receivers to be implemented, it is needed that the optical carrier power is larger than the peak power of the information signal (KK relations [40]). Such techniques involve DSP algorithms to overcome the SSBI degradation and it highly increases the network's complexity and cost [31].

In order to avoid the use of complex DSPs on short-reach networks as DCs, this work will focus on a new SSBI mitigation approach that can reduce the network cost and complexity. This innovative technique is based on transmitting separately the virtual carriers that are used to assist the detection in a dedicated core of the weakly-coupled MCF and the data signals are transmitted in the remaining cores of the MCF.

In Figure 2.4 it is shown a simplified diagram of the technique that this work will be focused on, where the SSBI component is created separately and then it is used to eliminate the SSBI component from the signal that contains the information to be retrieved.

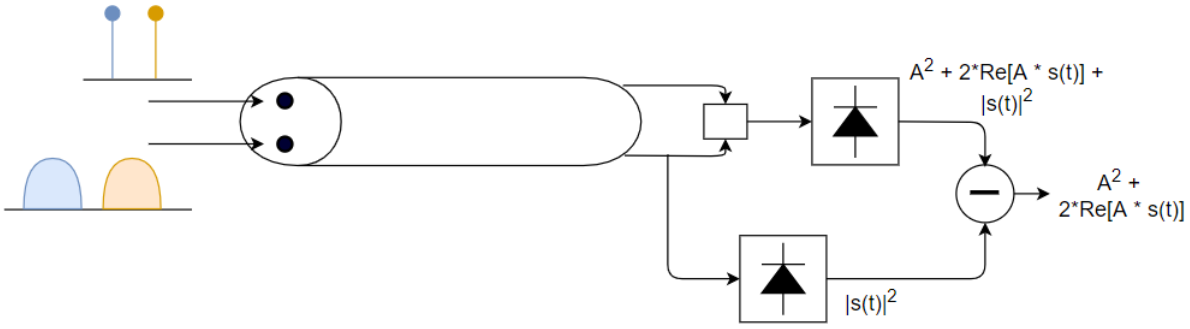

Figure 2.4: Proposed SSBI mitigation technique.

2.5 Conclusions

In this chapter, the main theoretical concepts related to this work were discussed. It has been seen that, in order to accommodate the continuous traffic growth observed in today's networks, changes in terms of power consumption and transmission capacity are needed, particularly in short-reach networks such as DCs. To face this problem, MCF-based SDM is pointed out as the most promising solution, enhancing the network

capacity and helping to manage the space limitations in intra DC communications. It has also been shown that weakly-coupled homogeneous MCF is identified as a solution for DC applications, since it requires a less complex architecture and for shorter distances the XT is less problematic to the system. Finally, in section 2.4, it was discussed the SSBI limitation that arises when DD receivers are employed. This impairment can severely degrade the system performance. To avoid using complex DSPs that would increase the system complexity and cost, a new transmission technique that enables a SSBI mitigation approach is proposed.

Chapter 3

Description of the system and impairments evaluation

In this chapter, the IM-DD optical system setup is described. In section 3.1, the system model under study is presented and the respective blocks (transmitter, MCF, receiver) are explained in detail. In section 3.2, the theory behind the impact of the laser phase noise, skew and chromatic dispersion effect on the system is described and the validation of the simulation model employed to emulate the laser phase noise is presented. The results until section 3.3 consider a back-to-back implementation. Finally, in section 3.3, the evaluation of the impact of the phase-to-intensity noise conversion on the NRZ signal is assessed using the eye-diagram and the eye-opening penalty as figure of merits.

3.1 Description of the IM-DD optical system setup

3.1.1 System model

Figure 3.1 presents an equivalent model of the proposed optical transmission system based on DD used to assess the performance of 200 Gb/s short-reach networks, as DCs, employing MCFs and the SSBI removal technique considered to mitigate the SSBI impairment. In the optical transmitter, the signal is generated apart from the virtual carrier. This virtual carrier is used to assist the detection at the receiver. The transmitter

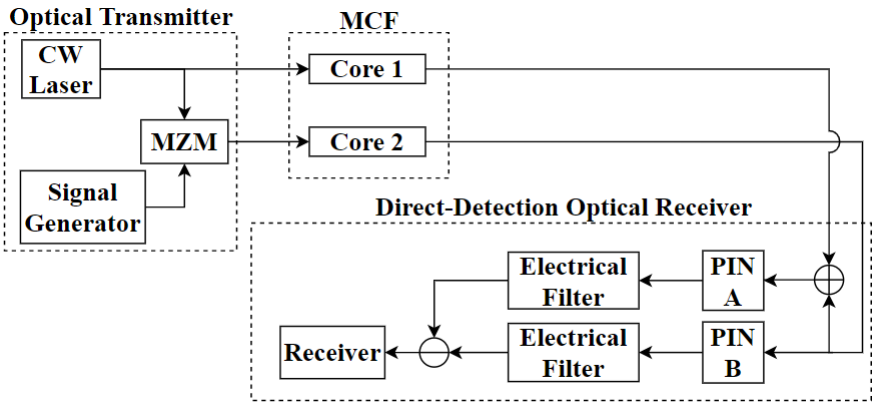

Figure 3.1: Scheme of the optical system employing DD and SSBI removal.

is responsible for converting the generated signal into the optical domain (electrical to optical conversion). Then, the outputs of the transmitter (the optical signal and the carrier) are transmitted separately into two different cores of the MCF. By transmitting the signal apart from the carrier, it is possible to estimate the SSBI component at the receiver. Transmitting the virtual carriers in a dedicated core and the data signals on the remaining cores is proposed to reduce the network cost and complexity. Then, after fibre propagation, the carrier and the NRZ signal are added before reaching the DD receiver. As Figure 3.1 shows, the DD-based receiver includes two positive-intrinsic-negative (PIN) photodetectors for the optical to electrical conversion, filtering to remove the out-of-band distortion and noise, and the SSBI removal block where the SSBI component is subtracted from the desired signal. In the following sections, these different blocks are discussed in detail.

3.1.2 Optical transmitter

The optical transmitter is responsible for the conversion of the electrical signal (obtained from the data bit sequence) to the optical domain. There are two options for the optical source: a light emitting diode (LED), that despite being low-cost has a high spectral linewidth and can only be properly used with low bit rates and for very short distances, and a laser diode, that has a much narrower spectral linewidth and can be used with high bit rates and for short and long distances.

The optical transmitter can employ direct or external modulation. External modulation is composed by a continuous wave (CW) laser source and an external modulator (as a MZM), presenting better performance and higher bandwidth although being more costly than direct modulation, which uses the current applied to the laser to control the

optical output power of the optical source. This last modulation scheme has the advantage of being low-cost, but have worse performance, high chirp and a lower bandwidth than external modulation. In this work, given these characteristics presented above, an optical transmitter that employs external modulation is used.

The external modulator used in this work is a single arm MZM that has negligible chirp, low optical loss and broad bandwidth [41]. The input-output characteristic of the MZM is given by [42]

$$\frac{e_{out}(t)}{E_{in}} = \frac{1}{\sqrt{i_l}} \cos\left(\frac{\pi}{2V_{sv}}\Big(-V_b + v_{ac}(t)\Big)\right) \tag{3.1}$$

where E_{in} is the input electrical field, i_l corresponds to the insertion losses, V_{sv} is the switching voltage of the modulator, V_b is the bias voltage of the modulator and $v_{ac}(t)$ represents the generated 200 Gb/s polar NRZ signal considered in this work. The electrical field at the output of the single arm MZM is denoted by $e_{out}(t)$.

The bias voltage of the modulator is used to control the bias point of the MZM. The MZM can be biased to any chosen point, being quadrature bias point (QBP) and minimum bias point (MBP) the most frequently chosen points. At QBP, an optical carrier is generated. Contrarily, an optical signal with suppressed carrier is achieved when the MZM is biased in the MBP. Since in this work the carrier is generated and transmitted separately from the signal, the MZM is biased at MBP where $V_b = V_{sv}$, in order to obtain a carrier-free signal.

Figure 3.2 shows the power spectral density (PSD) of the 200 Gb/s NRZ optical signal at the MZM output, and as it can be seen, the optical carrier is not generated.

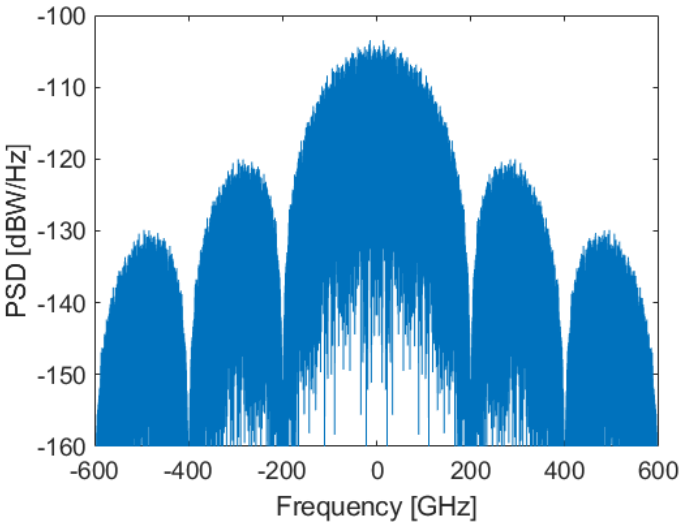

Figure 3.2: PSD of the NRZ signal at the MZM output.

3.1.3 MCF model

As depicted in Figure 3.1, the transmitter and the receiver are linked using a MCF. In this work, a MCF with two cores is considered: one of the cores is used to transmit the optical signal generated by the MZM and the other core is used to transmit the carrier. As this work is a preliminary study on the proposed transmission scheme and SSBI mitigation technique, in order to evaluate the impact of the skew and the laser phase noise, it is not needed to consider more than only one interfering core.

The fibre transmission results in distortion, attenuation and delay of the signals of the two cores. The transmission in each core is modelled by the following single mode propagation transfer function (that assumes linear propagation along the MCF)

$$H_f(\omega) = \exp\left(-j\beta_0 L - j\frac{1}{v_g}\omega L + j\frac{1}{2}\frac{\lambda_0^2 D_{\lambda_0}}{2\pi c}\omega^2 L - j\frac{1}{6}\left(\frac{\lambda_0^4 S_{\lambda_0}}{(2\pi c)^2} + \frac{\lambda_0^3 D_{\lambda_0}}{2\pi^2 c^2}\right)\omega^3 L\right) \cdot \exp\left(-\frac{\alpha}{2}L\right) \tag{3.2}$$

where β_0 involves the phase velocity, $\frac{1}{v_g} = \beta_1$ represents the propagation time delay per unit of length, λ_0 is the operating optical wavelength, D_{λ_0} is the dispersion parameter at the wavelength λ_0, S_{λ_0} is the slope of the dispersion parameter at the wavelength λ_0, c corresponds to the speed of light in vacuum ($c = 299792458$ m/s), ω is the angular frequency, L stands for the fibre length and α is the fibre attenuation coefficient. This coefficient is used in equation 3.2 in its equivalent Nepper/m form, given by

$$\alpha = \frac{\alpha_{\text{[dB/km]}}}{10^4 \log_{10} e} \tag{3.3}$$

where $\alpha_{\text{[dB/km]}}$ is the fibre attenuation coefficient in dB per km.

The fibre propagation in the two cores of the MCF causes a relative propagation time delay between cores, defined as the skew. In this work, the analysis of the skew effect in the retrieved signal is of primary importance. Taking the system architecture employed into account (see Figure 3.1), this delay will be crucial to determine if an accurate SSBI removal is achieved, since it strongly depends on the time relation between the optical carrier and NRZ signal that travels separately in the MCF before being added. To understand the practical effect of the skew on the signals injected in the fibre we need to refer to the fibre transfer function (equation 3.2) and in particular to β_1. By calculating β_1 from one core, the β_1 of the other core is obtained from the skew, which will be often used as a changing parameter in the simulation.

After imposing a certain skew value, the difference between the β_1 of each core, known as walkoff, is calculated as

$$\text{walkoff} = \frac{\text{skew}}{L} \tag{3.4}$$

Then, the difference between the propagation time delay is determined as follows

$$\beta_{1,2} = \beta_{1,1} - \text{walkoff} \tag{3.5}$$

where $\beta_{1,2}$ and $\beta_{1,1}$ are the propagation time delay of each core. Having defined each core's fibre propagation equation based on their different β_1, it is possible to evaluate any given relative propagation delay (skew) intended in order to investigate its impact on the SSBI removal technique effectiveness.

The parameters used to model the fibre transmission are presented in Table 3.1, according to ITU-T recommendations [43].

Table 3.1: Parameters used in the SSMF transfer function.

ν_0 [THz]	193.1
λ_0 [nm]	1552.52
α [dB/km]	0.21
D_{λ_0} [ps/nm/km]	18
S_{λ_0} [fs/nm^2/km]	90

The transmission of the signal is made in the C-band (conventional band from 1530 nm to 1565 nm), where today's optical fibers present its lowest loss values.

3.1.4 Optical receiver

After transmitting the data through the MCF, the signal and the carrier reach the direct-detection optical receiver. At this point, the NRZ signal is added to the carrier in one branch, and in the other branch remains only the signal (see Figure 3.1). Figure 3.3 shows the PSD of the carrier-added signal at the receiver input, with no skew considered. As Figure 3.3 shows, contrarily to Figure 3.2, the spectral line of the carrier can be noticed at the frequency of 0 GHz.

Once the signals are organised as intended, it is converted into the electrical domain. This is done by a photodetector that converts optical power into electric current

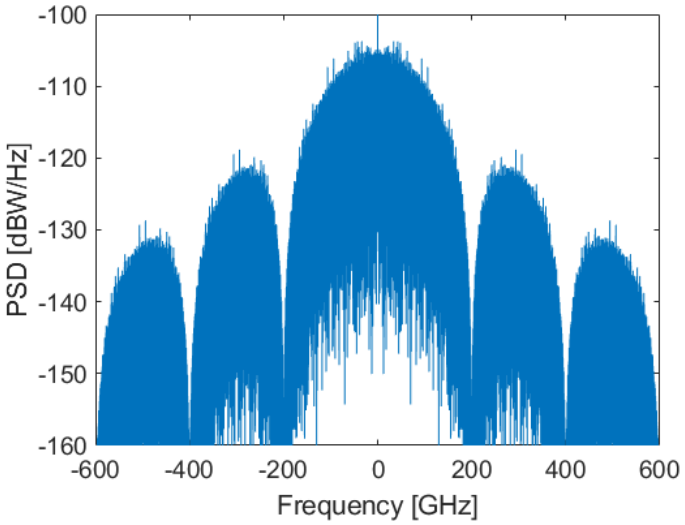

Figure 3.3: PSD of the NRZ signal with the carrier at the optical receiver input.

through the photoelectric effect [44]. There are two commonly used semiconductor photodiodes, the PIN photodiode and the avalanche photodiode (APD). The ADP has an internal gain and high sensitivity, but in contrast it has high cost and a complex structure. The PIN photodiode, on the contrary, presents a simple structure and has a low-cost, which is highly preferable for most systems, including the proposed in this work. The DD-based receiver uses a PIN, and the expression that gives the signal at the output of this PIN can be written as:

$$i_{PIN}(t) = R_\lambda \cdot |e_{PIN}(t)|^2 + n_e(t) \tag{3.6}$$

where $|e_{PIN}(t)|^2$ is the instantaneous power of the optical signal at the input of the PIN and $n_e(t)$ represents the electrical noise generated. In the case of the PINs presented in Figure 3.1, the optical signal at the PIN input can be the carrier added with the NRZ signal or the NRZ signal alone. R_λ is the PIN responsivity given by [44]:

$$R_\lambda = \frac{\eta q}{h\nu} \quad \text{[A/W]} \tag{3.7}$$

where η is the PIN efficiency, q is the electron charge, ν corresponds to the optical frequency of the input signal and h is the Planck's constant. For the studies of this work, a PIN responsivity of $R_\lambda = 1$ A/W was considered.

After photodetection, the signal passes through an equivalent model of the electrical filter, that is used to selectively filter an information-bearing signal from undesired impairments such as noise and interference. In this work, a Bessel low-pass filter is

considered, that has a transfer function given by [45]

$$H(f) = \frac{d_0}{B_n(s)} \tag{3.8}$$

with

$$s = \frac{jf\sqrt{(2n-1)\,ln2}}{B_{-3\,\text{dB}}} \tag{3.9}$$

where $B_{-3\,\text{dB}}$ is the -3 dB bandwidth of the filter and $B_n(s)$ is the n-th order Bessel polynomial given by

$$B_n(s) = \sum_{k=0}^{n} d_k\, s^k \tag{3.10}$$

with

$$d_k = \frac{(2n-k)!}{2^{n-k}k!(n-k)!} \tag{3.11}$$

3.1.5 Eye-diagram evaluation

After processing the signal through the PIN and electrical filter, the eye-diagram can be used for performance evaluation, since it enables the visualisation and estimation of the impact of the distortion and noise effects on the received bits. Figure 3.4 shows the eye-diagram of the NRZ signal after filtering, considering a third-order Bessel filter with a $B_{-3\,\text{dB}}$ of 160 GHz, with no skew considered nor electrical noise addition (reference/ideal scenario).

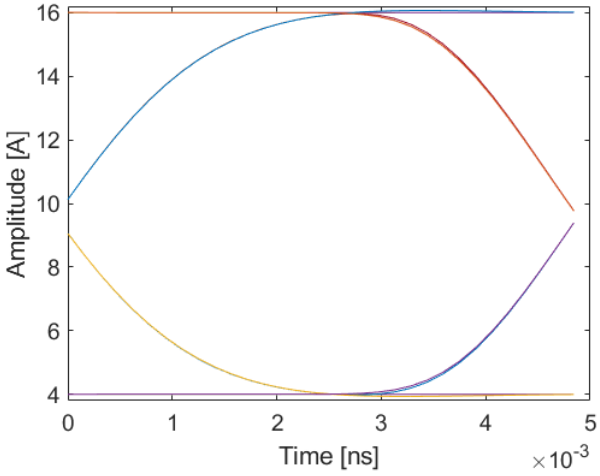

Figure 3.4: Eye-diagram of the NRZ carrier-added signal in ideal transmission conditions after electrical filtering.

As depicted in Figure 3.4, the eye is completely open, taking into account the ideal

transmission conditions of the system assumed so far. The results obtained in these conditions can be used as a reference situation to assess the affects of the impairments considered throughout this work (particularly in section 3.3).

One method to obtain a fast estimation of the signal quality from the eye-diagram is the eye-opening penalty (EOP). This can reflect the signal distortion and eye closure due to noise effects. The formula to calculate the EOP is given by

$$EOP = -10 \cdot \log_{10}\Big(\frac{I_1 - I_0}{2I_{av}}\Big) \quad [\text{dB}] \tag{3.12}$$

where I_1 represents the lowest current level associated with bits 1 and I_0 represents the highest current level associated with bits 0. The values of I_1 and I_0 are taken at the time instant for which the eye-diagram opening is maximum. I_{av} is the average current given by

$$I_{av} = (P_s + P_c) \cdot R_\lambda \tag{3.13}$$

where P_s is the NRZ signal mean optical power and P_c is the carrier mean optical power at the PIN input. Since it is considered a responsivity of 1 A/W, $2\,I_{av}$ represents the greatest eye-opening that can be obtained. For this ideal case, $I_1 - I_0$ is equal to $2\,I_{av}$ and the EOP is 0 dB.

From this point on, further EOP calculations and eye-diagrams can be compared to this (reference) scenario so the obtained results reflect the penalty that is induced in the system by other impairments, namely, the laser phase noise and the skew between cores.

3.1.6 SSBI removal block

This subsection describes how the SSBI component is obtained in the receiver and then used to recover the SSBI-free desired signal. Based on equation 3.6 (neglecting the electrical noise for this demonstration purpose), it is possible to write the photocurrent at the output of each PIN, by substituting $e_{PIN}(t)$ by the optical field at its input.

Regarding the carrier, as it is a constant wave it does not vary over time, so it can be represented as A_c, corresponding to its amplitude. The current at the output of PIN A in Figure 3.1 is given by

$$i_A(t) = A_c^2 + 2 \cdot A_c \cdot \Re\{s_2(t)\} + |s_2(t)|^2 \tag{3.14}$$

where $s_2(t)$ is the information signal at the input of PIN A. The first term of equation 3.14 is a DC component, the second term is the desired 200 Gb/s NRZ signal and the last term represents the SSBI component. Figure 3.5 shows the PSD at the PIN output, where the SSBI term, $|s_2(t)|^2$, is highlighted.

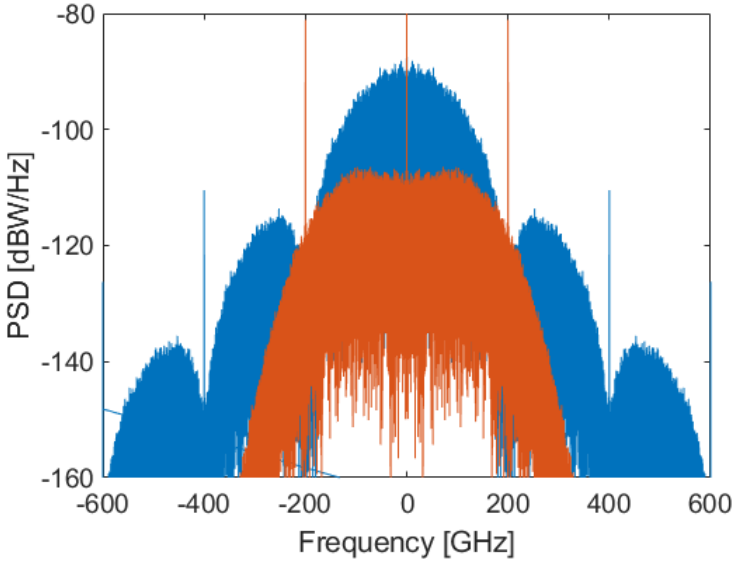

Figure 3.5: PSD of the signal and corresponding SSBI term (in orange).

As Figure 3.5 illustrates, the SSBI component is generated and is overlapped in the same frequency range as the signal, undermining the quality of the wanted to retrieve signal. This SSBI removal block is implemented to mitigate this impairment. To do so, the SSBI term is obtained by photodetecting the signal separately from the carrier:

$$i_B(t) = |s_2(t)|^2 \tag{3.15}$$

and then use it to subtract this term from the wanted signal photocurrent (equation 3.14), resulting in the following expression

$$i_{final}(t) = i_A(t) - i_B(t) = A_c^2 + 2 \cdot A_c \cdot \Re\{s(t)\} \tag{3.16}$$

where the DC component (first term) is removed with a DC block, remaining the desired signal which contains the data to be retrieved.

3.2 Theoretical analysis of the skew, laser phase noise and dispersion effects on the signal

In optical communications, the laser phase noise, that portrays how the phase of a laser diverts from an ideal sinusoidal wave [46], is a relevant impairment of the system and it is necessary to understand its behaviour in order to correctly estimate its impact on the system performance. In an ideal situation, where the laser phase noise is not considered, the electrical field at the laser output can be represented as follows

$$e_0(t) = A\, e^{j\phi_0} \tag{3.17}$$

where *A* is the amplitude of the continuous wave and ϕ_0 represents the phase at the time origin (*t*=0). This would generate a line in the electrical field PSD with null spectral linewidth. However, in a real optical source, the electrical field is represented as

$$e_0(t) = \big(A + n_a(t)\big)\, e^{j\phi_0} e^{j\phi_n(t)} \tag{3.18}$$

where $n_a(t)$ is the amplitude noise of the optical source and $\phi_n(t)$ represents the phase noise of the optical source that appears due to the spontaneous emission effect. The PSD of the $\phi_n(t)$ is directly related to the laser linewidth, $\Delta\nu_L$, and it is calculated as follows [47]

$$S_{\phi_n(t)} = \frac{\Delta\nu_L}{2\pi} \tag{3.19}$$

This leads to lasers with a output field PSD that is no longer represented by a line with null spectral linewidth. This phase fluctuation of the laser, that can be quantified by its linewidth, is modelled by a Wiener process [48]. A Wiener process can be obtained from the integral of a white noise Gaussian process, described by [49]

$$\phi_n(t) = 2\pi \int_0^t n(t)\, dt \tag{3.20}$$

where *n(t)* is a zero mean stationary white Gaussian random process. The expression 3.20 is used as a model in the simulator to obtain the laser phase noise.

3.2.1 Laser phase noise model validation

In this subsection, the results obtained from the simulator model and the considered phase noise theoretical model are compared. In Figure 3.6, it is possible to view four phase noise samples for a laser linewidth of 100 kHz, where each sample shows the randomness of the phase noise amplitudes, that are independent from sample to sample. These results can be described as a continuous Brownian motion with zero mean and a variance of $2\pi\Delta\nu_L t$, corresponding to a Wiener process.

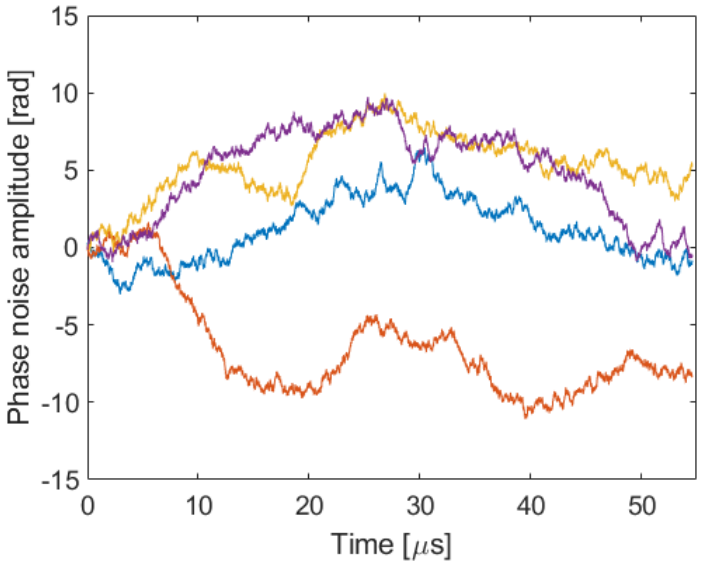

Figure 3.6: Four independent phase noise samples for a laser linewidth of 100 kHz.

Figure 3.7 presents the PSD of the electrical field at the output of the laser for linewidths of 100 kHz, 500 kHz, 1MHz and 10 MHz. This linewidth is measured at -3 dB of the peak, i.e., half power of the maximum PSD of the electrical field at the laser output. Each sub-figure of Figure 3.7 presents the theoretical and simulation results for the laser linewidths under study. The theoretical results were obtained by a Lorentzian function given by

$$l = \frac{1}{1 + \frac{f^2}{\left(\frac{\Delta\nu_L}{2}\right)^2}} \tag{3.21}$$

where f represents the frequency where the Lorentzian function (l) is being calculated.

It can be noticed that in each plot occur very good agreement between the PSD spectra of the laser field obtained in simulation and the theoretical curve, validating the laser phase noise simulator model used in this work.

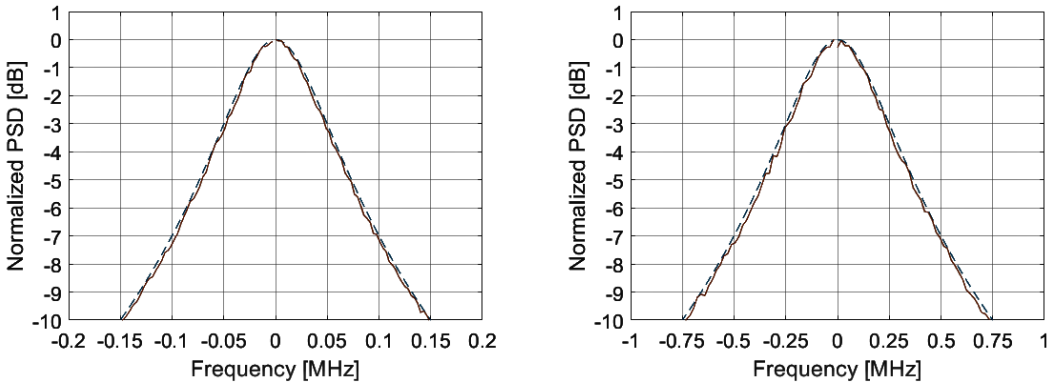

(a) 100 kHz linewidth

(b) 500 kHz linewidth

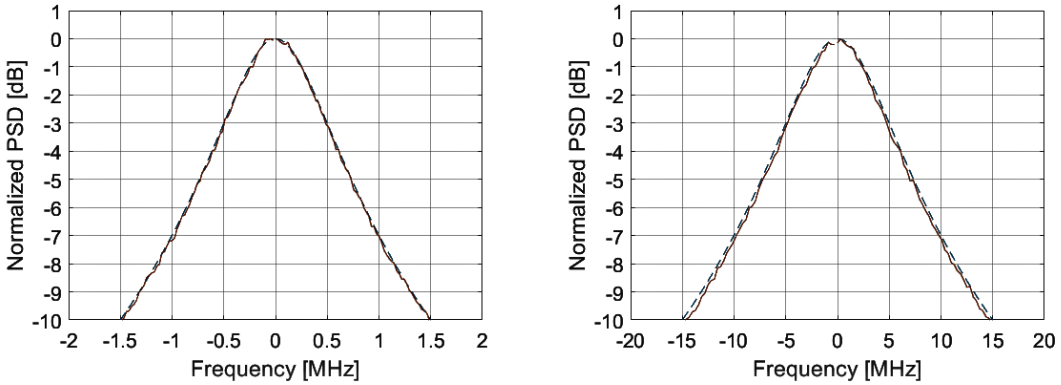

(c) 1 MHz linewidth

(d) 10 MHz linewidth

Figure 3.7: PSD of the laser phase noise for different linewidths: Simulation (continuous line) and theoretical (dashed line) results.

3.2.2 Skew, laser phase noise and dispersion effects on DD systems

The relation between the skew and the laser phase noise coherence time, t_c, can provide a solid estimation about how the skew may impact the system performance due to phase noise. The laser phase noise coherence time is given by [50]

$$t_c = \frac{1}{\pi \cdot \Delta v_L} \tag{3.22}$$

If we consider the laser electric field at two different time instants, t and $t+T$, the coherence time can be defined as the maximum T value for which the phase difference between the electric field at the two time instants remains predictable [50]. Since the DD receiver photodetects each signal through a PIN photodiode, the current associated with the carrier-added data signal (output of PIN A), considering the skew and the laser phase noise, can be written as:

$$i_A(t) = \left| A_c\, e^{j\phi_n(t)} + s(t-T_s)\, e^{j\phi_n(t-T_s)} \right|^2 \tag{3.23}$$

where $s(t)$ is the data signal at the MCF output and T_s is the skew between cores. If t_c is much longer than the skew, the degradation caused by the phase noise is small since the relative delay time between the two cores leads to a situation where, at a given time instant, the phase noise at the output of the two cores has similar amplitudes. In this case, when the carrier is added to the signal, no destructive interference occurs. Based on equation 3.23, the aforementioned relation between t_c and the skew can be mathematically expressed. If the skew is much shorter than t_c, then

$$e^{j\phi_n(t-T_s)} \approx e^{j\phi_n(t)} \tag{3.24}$$

resulting for the current at the output of PIN A:

$$i_A(t) \approx \left|\big(A_c + s(t-T_s)\big)\cdot e^{j\phi_n(t)}\right|^2 = \left|A_c + s(t-T_s)\right|^2 \tag{3.25}$$

In this case, the received signal is not impaired by the laser phase noise and it is possible to successfully eliminate the SSBI component (equation 3.15) and then obtain the SSBI-free signal. As opposed, in the scenario where t_c is not sufficiently longer than the skew, equation 3.24 is not verified and so the phase noise is not eliminated when the signal is photodetected, causing phase-to-intensity noise conversion, which will be analysed further on.

One of the main goals of this work is to identify the conditions under which a negligible degradation due to the combined effect of the skew and the laser phase noise is obtained. When the degradation due to the combined effect of the skew and the laser phase is negligible, the current at the output of PIN A is given by:

$$i_A(t) = A_c^2 + 2\cdot A_c \cdot \Re\{s(t-T)\} + |s(t-T)|^2 \tag{3.26}$$

In this scenario, there are two major impairments that can cause performance degradation: the SSBI (last term) and the chromatic dispersion. The delay, T, is due to the propagation and can be compensated without causing distortion. The dispersion effect is represented in the term $s(t)$ as follows

$$s(t) = s_{in}(t) * h(t) \tag{3.27}$$

where $s_{in}(t)$ is the data signal at the MCF input, "$*$" is the convolution operator and $h(t)$

is the impulse response of the SM fibre, which contains the attenuation and dispersion effects of the MCF. It is possible to electronically remove the dispersion effects through DSP techniques. However, this can be performed only after the SSBI term is removed. The dispersion impact on the system performance is assessed in section 4.3.

3.3 Evaluation of the impact of the skew and laser phase noise on the NRZ signal EOP

Before analysing the impact caused by the skew on the phase-to-intensity noise conversion, it must be assured that the numerical results are obtained in valid simulation-wise conditions. Firstly, a valid simulation window, T_W, is required. This time window indicates the total time needed to represent the bits generated on the program and the corresponding samples per bit. T_W must always be higher than the skew value under evaluation on the simulator. Not fulfilling this requirement means that the skew can be of the same magnitude order as T_W. In an extreme example case, if the skew is exactly the same as T_W, it would result in having each bit sample in the same vector position when comparing the signal vector at the fibre output with the input. This could represent a simulation problem since it would not reflect any degradation caused in the system regarding to what concerns to the skew impact on the phase-to-intensity noise conversion, which would not be in accordance with reality. This validation needs to be done since in the simulator the fibre delay is emulated with a circular shift, where the bits samples are dislocated from their vector position. This way, it is avoided that the circular delay performs a full circular motion, resulting in an unchanged signal vector.

To evaluate the impact of the laser phase noise on the NRZ signal and its variation with the skew, a study based on the EOP and eye-diagrams at different points of the 200 Gb/s NRZ optical communications system has been done. Figure 3.8 shows the system points where the eye-diagrams were obtained.

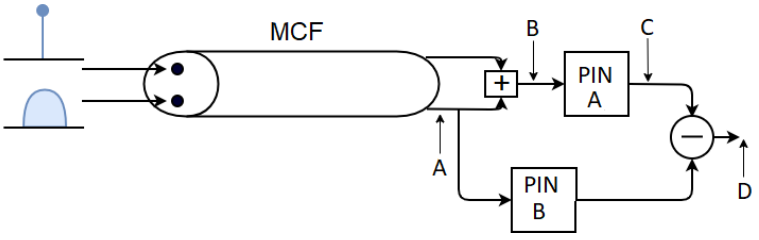

Figure 3.8: Eye-diagram evaluation points.

As it is shown in Figure 3.8, the carrier and the signal are transmitted in separate cores and to obtain the results presented in this subsection, we have considered the mean optical power at the input of each core set to 0 dBm. The MCF length is set to 2 km.

To assess the impact that the skew has on the EOP, the relation between the skew and t_c and how this relation affects the eye-opening penalty was studied. Figure 3.9 and 3.10 show the mean EOP values taken for a skew of 10 ns and 50 ns, after SSBI removal (evaluation point D in Figure 3.8). In each run, the variation that can occur in the EOP values is caused by the laser phase noise and its inherent randomness, so it is important to calculate a mean value in order to evaluate at which point the fluctuations in the EOP values becomes minimal. This mean value is calculated after each transmission, by obtaining the corresponding EOP and averaging it with all values collected to that moment. These results were obtained for a laser linewidth of 1 MHz (which results in a t_c of 318.3 ns). For the skew of 10 ns, the simulation was done with 2^{15} bits which leads to a T_W of 164 ns. For the skew of 50 ns, 2^{16} bits were employed which originates a T_W of 327.7 ns. Thus, the simulation time window is at least 6 times longer than the skew.

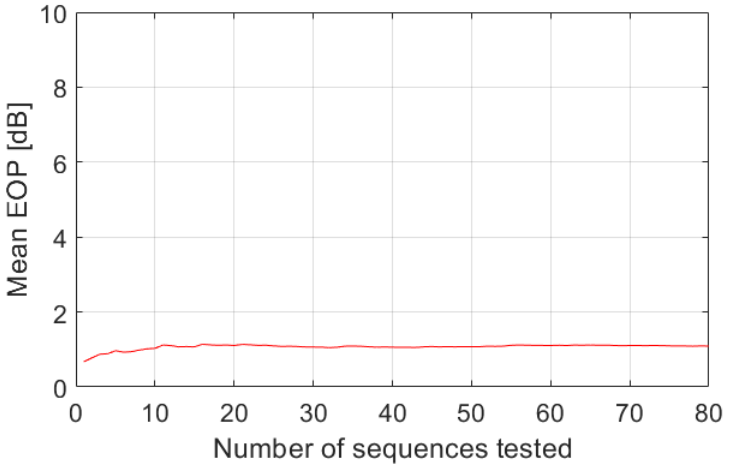

Figure 3.9: Mean EOP as a function of the number of sequences tested with skew of 10 ns.

From Figure 3.9, it is possible to confirm that the degradation induced by the laser phase noise is not too significant (approximately 1 dB EOP), comparing with the reference situation in subsection 3.1.5, which is explained by the fact that the phase noise coherence time is much longer than the skew (approximately 30 times higher) and so destructive interference is not caused when adding the signal with the carrier. As the evolution of the mean EOP with the number of tested sequences show, the results

obtained present low variation and the curve stabilizes rapidly around 10 sequences tested, due to the low impact of the phase noise on the NRZ signal.

Contrarily, Figure 3.10 shows the high penalty (comparing to Figure 3.9 and to the scenario exposed in subsection 3.1.5) and fluctuation that occurs when the coherence time is not long enough comparing with the skew (in this case, t_c is only 6 times longer than the skew). In cases like the latter (Figure 3.10), the eye-opening penalty is highly influenced by the phase-to-intensity noise conversion and, taking into account the randomness associated with the phase noise process, the results can vary significantly from one sequence to another, and for this reason it is even more important to calculate a mean EOP.

Figure 3.10: Mean EOP as a function of the number of sequences tested with skew of 50 ns.

As shown in Figure 3.10, the curve of mean EOP almost stabilizes around 30 sequences. From this point on, the EOP will be calculated as a mean EOP from at least 30 tested sequences.

Another form of visualizing the impact of the noise effects on the signal is through the eye-diagram, which gives a rapid and simple estimation of the degradation induced on the bits of the time waveform. Figure 3.11 shows the signal at point A, before adding the carrier (point B). Since the MZM at the transmitter is operating at MBP and a polar signal is used, the amplitudes of the field for bits 1 and 0 are identical, and the corresponding eye-diagram is totally closed.

At point A, the eye-diagram is the same for any laser linewidth and skew chosen because since it is being represented the amplitude of the optical field. There is no representation of the phase-to-intensity noise conversion, since it only occurs after photodetection.

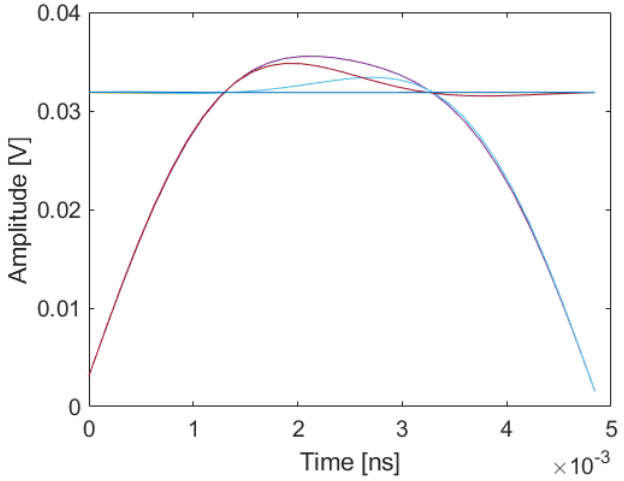

Figure 3.11: Eye-diagram at point A of the system.

Figures 3.12 and 3.13 show the eye-diagrams at points B and C, respectively. In point B, the optical carrier is added to the NRZ signal and the eye-diagram of the amplitude of the optical field presents a visible alteration. After adding the carrier and the data signal, the resulting signal is photodetected by a PIN (point C). At point C, the undesired SSBI component is originated.

As Figure 3.12 shows, the chosen laser linewidth can significantly impact the NRZ signal. In Figure 3.12, it is possible to see the major difference in the eye closure between the situation with the laser phase noise generated from the 100 kHz linewidth laser compared to the 5 MHz linewidth. After photodetection (Figure 3.13 - point C), it can be seen that for the 100 kHz linewidth, a skew of 5 ns does not cause significant eye closure, as opposed to the 5 MHz linewidth, where the photodetection process leads to severe phase-to-intensity noise conversion.

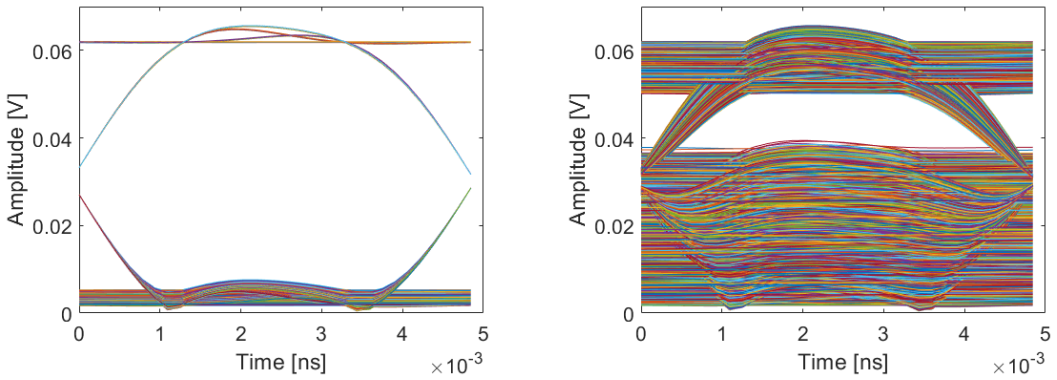

(a) 100 kHz linewidth (b) 5 MHz linewidth

Figure 3.12: Eye-diagram at point B of the system (skew of 5 ns).

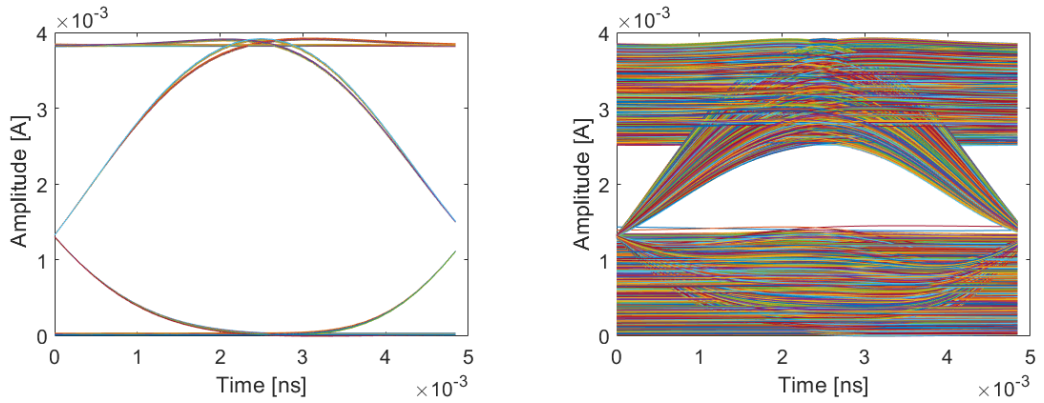

(a) 100 kHz linewidth (b) 5 MHz linewidth

Figure 3.13: Eye-diagram at point C of the system (skew of 5 ns).

As it is explained in the SSBI removal subsection (subsection 3.1.6), this work proposes a SSBI mitigation technique that is based on photodetecting the signal without the optical carrier, in order to estimate the SSBI component separately and then use it to remove the SSBI from the desired signal. Figure 3.14 shows the eye-diagram at point D of the system, where the SSBI component is subtracted from the carried-added NRZ signal.

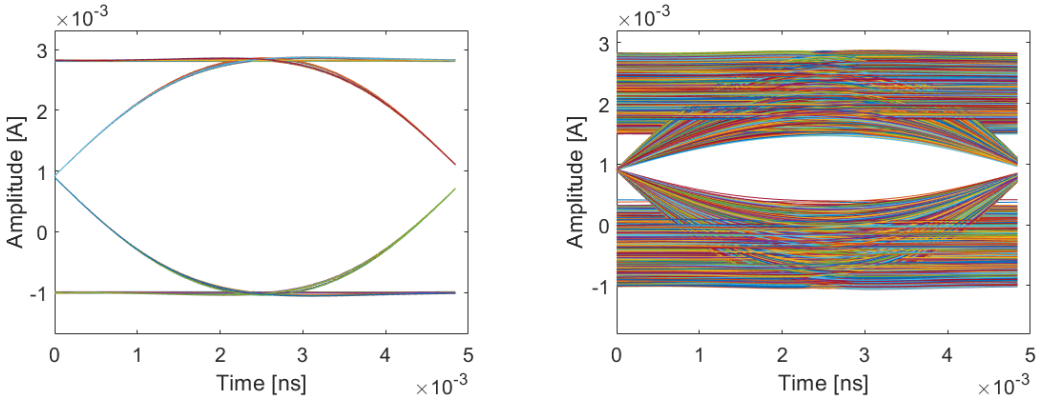

(a) 100 kHz linewidth (b) 5 MHz linewidth

Figure 3.14: Eye-diagram at point D of the system (skew of 5 ns).

As Figure 3.14 A) shows, when the skew is much shorter than t_c, which occurs for the laser linewidth of 100 kHz, the laser phase noise does not impact the eye-diagram considerably and the SSBI-free signal can be recovered. In contrast, the situation where t_c is not sufficiently longer than the skew is depicted in sub-figures B from Figures 3.12 to 3.14. Under this condition, the combined effect of the skew and the laser phase noise significantly impacts the eye-diagram. The scenario represented in Figure 3.14 B) illustrates the effects on the signal when equation 3.24 is not verified. In this case, the laser

phase noise component is not eliminated when the signal is photodetected, resulting in phase-to-intensity noise conversion. Due to the randomness of the phase noise, specially when the combined effect of the skew and the laser phase noise is significant, the obtained eye-diagrams can vary significantly from transmission to transmission. This highlights the importance of calculating the EOP as an average from multiple transmissions when quantifying the impact of the impairments in terms of eye-opening penalty.

To complete the eye-diagram impact study, Figure 3.15 presents the eye-diagrams in point D, for a 1 MHz laser linewidth.

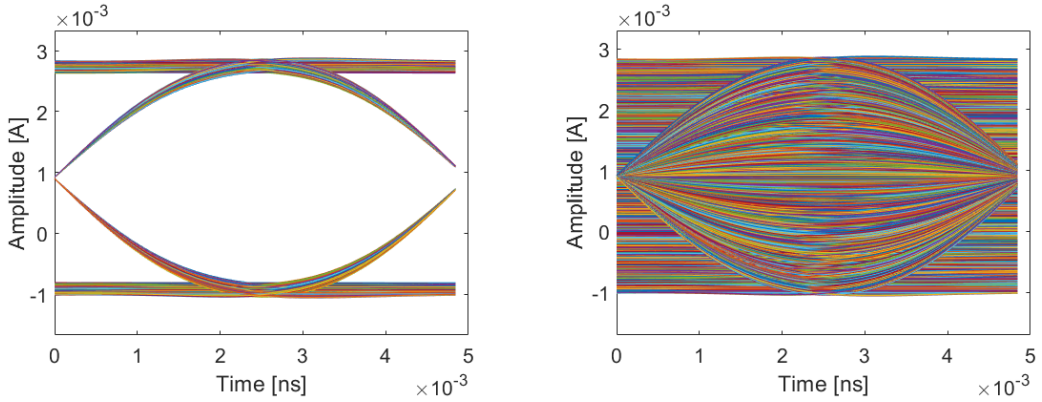

(a) 5 ns (b) 100 ns

Figure 3.15: Eye-diagram at point D of the system (laser linewidth of 1 MHz).

For the laser represented in Figure 3.15 (1 MHz linewidth), a skew of 5 ns is much shorter (approximately 60 times shorter) than the laser phase noise coherence time but on the other hand a skew of 100 ns is only 3 times shorter. As the results show, the eye-diagram degradation due to the laser phase noise is only significant when the coherence time is not longer enough than the skew.

The results obtained throughout this section demonstrate the high dependence of the system performance on the laser linewidth and the relative delay between the two cores of the MCF. By increasing the linewidth, the respective t_c decreases and the performance becomes more sensitive to shorter skew values. As the results have shown, a laser linewidth of 100 kHz can tolerate a skew value of 100 ns, whereas the 5 MHz linewidth laser is highly impacted by a 5 ns skew.

To summarize the study on the impact of the skew on the NRZ signal, Figure 3.16 presents the EOP values as a function of the skew for four different laser linewidths, before employing SSBI mitigation (point C). The results were obtained in electric noise free environment, focusing only on the effects caused by the skew and the phase noise.

Figure 3.16 shows that, increasing the linewidth values, the system becomes less

tolerable to a certain skew value, leading to a higher eye-opening penalty. The 0 Hz linewidth represents the reference situation, where the skew value is indifferent due to the absence of the laser phase noise, thus not degrading the signal received. The 5 MHz linewidth is not represented in Figure 3.16 since from a skew of 5 ns, due to the high impact of the phase-to-intensity noise conversion, in some transmissions the eye is totally closed, resulting in a EOP value of infinite. This leads to a mean EOP (mean value over 30 transmissions, as detailed before) value equal to infinite, therefore it is not possible to represent the corresponding curve.

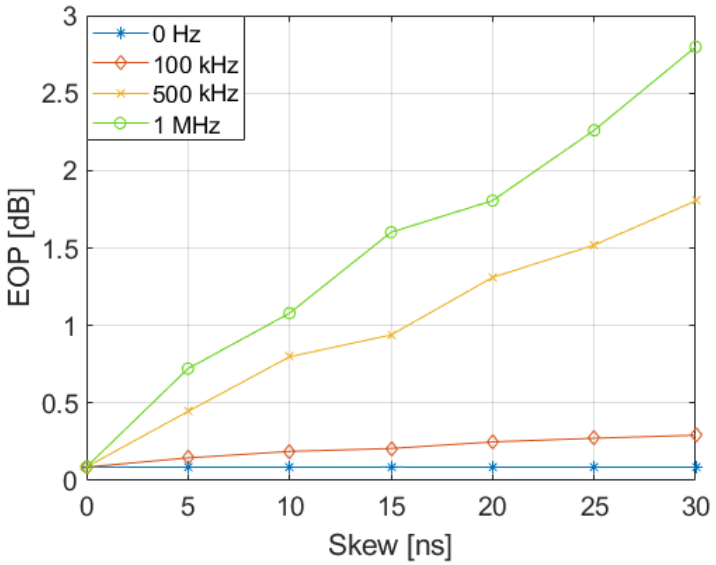

Figure 3.16: EOP as a function of the skew for different linewidths.

3.4 Conclusions

In this chapter, the 200 Gb/s NRZ optical communications system based on DD was described. The optical transmitter that converts the NRZ signal into the optical domain and generates the virtual carrier, the MCF model and the optical DD receiver constituted by two PIN photodetectors were discussed. The proposed SSBI mitigation technique was detailed, showing that it may effectively remove the SSBI term from the signal that contains the data to be retrieved. In section 3.2, the impact of the laser phase noise, skew and dispersion effects on these kind of DD-based MCF systems was discussed. Then, in section 3.3, the evaluation of the combined effect of the skew and the laser phase noise on the performance of the NRZ signal was assessed. The results showed that broader laser linewidths are less tolerable to a certain skew value, reflecting in higher

levels of phase-to-intensity noise conversion and thus a higher eye-opening penalty. The results obtained considered a mean optical power at the input of each core set to 0 dBm, focusing mainly on the penalty induced in the system by phase-to-intensity noise conversion.

Chapter 4

Performance evaluation of the DD MCF system

In this chapter, the performance of the proposed transmission scheme in short-reach networks using the system model described in Chapter 3 is assessed through numerical simulation. The proposed transmission scheme is mainly impaired by the combined effect of the skew, laser phase noise and chromatic dispersion of the optical fibre. The impact of those impairments is evaluated through EOP calculations and then through BER calculations (BER method detailed in Appendix B), using Monte Carlo numerical simulation. In section 4.1, the beneficial conditions to employ the proposed SSBI mitigation approach are presented. In section 4.2, the impact of the phase-to-intensity noise conversion due to the skew between cores on the system performance is evaluated. In section 4.3, the impact of chromatic dispersion on the system performance is quantified, to emulate as near as possible a real scenario, considering all impairments in combination.

4.1 Assessment of beneficial conditions for SSBI removal

The proposed transmission scheme leads to a relative delay between the carrier and the data signal which, as seen in Figure 3.16, impacts differently the system performance depending on the laser linewidth. This phase-to-intensity noise conversion may affect the effectiveness of the SSBI mitigation. Moreover, the received signal is also impaired

by the chromatic dispersion of the fibre. As the proposed transmission technique enables a low-complexity SSBI mitigation approach, the study of the conditions where this approach is effective is needed. This SSBI mitigation is required specially if electrical compensation of the dispersion is needed at the receiver side. From equation 3.26, we conclude that the impact of the SSBI term depends on the ratio between the carrier mean optical power and the signal mean optical power.

Figure 4.1 shows the EOP as a function of the relative power level, P_r, defined as the difference between the signal mean optical power (P_s) and the carrier mean optical power (P_c). The results were obtained with and without considering electrical noise, and for $P_c = 0$ dBm. The electrical noise is obtained following the method described in Appendix A.

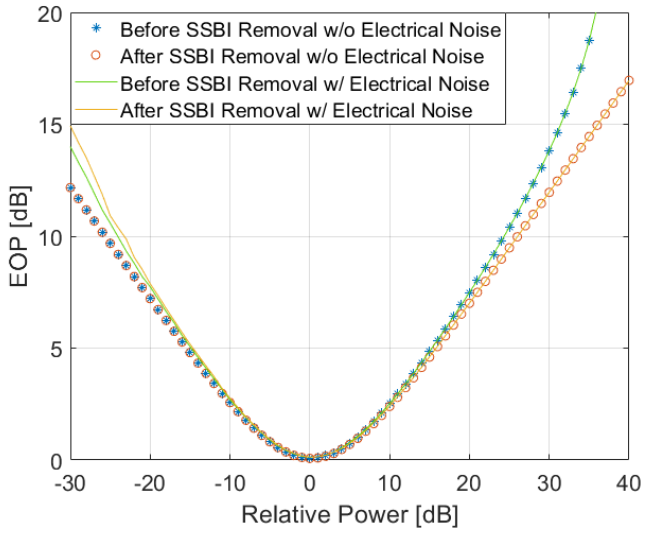

Figure 4.1: EOP as a function of the relative power level, before and after SSBI removal, with and without electrical noise.

When the relative power is lower than 0 dB, the EOP reflects the eye-closure due to the lowering of P_s values. It is also seen that, under these conditions, removing the SSBI can worsen the results, in the presence of electrical noise. This happens because when subtracting the output of PIN B from the output of PIN A, in fact two random and independent noise components with the same power are being added. On the other side, for P_r higher than 0 dB, the SSBI removal may lead to improvement of EOP. In this study, for high P_r values, the SSBI term is dominant over the electrical noise power considered, and so the electrical noise does not affect the retrieved signal in terms of the EOP in a visible manner.

As the results in Figure 4.1 show, although the implementation of the SSBI mitigation technique only shows beneficial for high P_r values, the optimum operation point is obtained for a relative power of 0 dB, i.e., when the NRZ signal and the carrier present the same mean optical power. As it was discussed in section 3.2, in a real-use scenario, the retrieved signal is also impaired by the dispersion. With this in mind, a study is conducted to understand the impact of the dispersion effects on the performance of the system operating at the identified ”ideal point”. Figure 4.2 shows the EOP as a function of the MCF length, for different laser linewidths, with and without dispersion and for $P_r = 0$ dB. The walk-off considered between cores is the parameter used in the simulator (equation 3.4) instead of the skew.

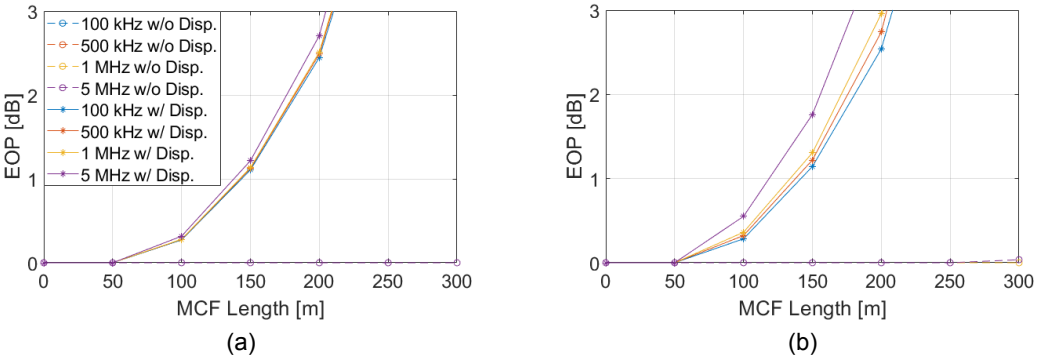

Figure 4.2: EOP as a function of the MCF length for different laser linewidths, with and without dispersion, for: (a) a walk-off of 1 ns/20 km and (b) a walk-off of 10 ns/20 km.

As shown in Figure 4.2, the dispersion clearly constrains the system even if working in the ideal situation (where P_r is 0 dB), showing a minimum of 2.5 dB penalty for all laser linewidths, for distances higher than 200 m. For both walk-off values studied, the dispersion is the main impairment responsible for the degradation, but it is noticeable that increasing the walk-off increases slightly the EOP. This happens because increasing the walk-off originates a higher skew for a given distance, and then the combined effect of the skew and the increasing laser phase noise (broader linewidths) leads to an additional performance penalty due to phase-to-intensity noise conversion. From the results in Figure 4.2, it is possible to conclude that even if considering the relative power level that represents the ”ideal” operation point (identified in Figure 4.1), when introducing other impairments, in particular the dispersion, the system is highly degraded by it. Results in Figure 4.2 show that the dispersion effect overcomes all other impairments considered (electrical noise, skew and phase noise), thus being the most significant. For this reason, if system performance improvement is required, dispersion

needs to be fully compensated. As shown in equation 3.26, for the dispersion to be compensated electronically at the receiver side, the SSBI term needs to be successfully mitigated beforehand. It was seen in Figure 4.1 that an efficient SSBI mitigation may only occur for high P_r. A similar study to the one presented in Figure 4.1, now considering the BER as the performance metric, is carried out, in order to detail the effectiveness of the SSBI mitigation technique under the different conditions discussed. Electrical noise is considered, but now (and from this study onwards) it is categorised by the electrical signal-to-noise ratio (SNR) defined as

$$SNR = \frac{P_{tot}}{P_{noise}} \tag{4.1}$$

where P_{tot} is the average power of the electrical signal resulting from the carrier-added NRZ signal photodetection (by PIN A) and electrical filtering and P_{noise} is the noise power at the electrical filter output. From equation 4.1, given a certain SNR value under test and the mean power of the received signal imposed by P_{tot}, P_{noise} is determined and used to simulate the noise component added after photodetection in both branches (PIN A and B). The electrical noise is now simulated through this approach in order to understand the influence of the noise levels on the SSBI estimation and mitigation process.

Before choosing which SNR values to use in the following studies, it must first be assessed the maximum SNR value, SNR_{max}, that can be achieved for the typical noise levels observed in receivers. To calculate the minimum noise power P_{noise} that can be obtained at the output of the electrical filter of the PIN, for a receiver with a very high sensitivity, we consider a square root of the PSD of the current noise of $\sqrt{S_c} = 10^{-12}$ A/$\sqrt{\text{Hz}}$. Then, P_{noise} is given by (considering a 1 Ohm electrical resistance)

$$\begin{aligned} P_{noise} &= \left(\sqrt{S_c} \cdot \sqrt{B_{e,n}}\right)^2 = \left(10^{-12} \cdot \sqrt{1.62 \times 10^{11}}\right)^2 \text{ A}^2 \\ &= 1.62 \times 10^{-13} \text{ W} \approx -98 \text{ dBm} \end{aligned} \tag{4.2}$$

where $B_{e,n}$ is the noise equivalent bandwidth of the electrical filter of the optical receiver (detailed in Appendix A). Considering a signal and carrier mean optical power set to 0 dBm at the input of the fibre, at PIN A output we obtain $P_{tot} \approx$ -31 dBm. Resorting to equation 4.1, SNR_{max} is determined

$$SNR_{max} = -31 - (-98) = 67 \text{ dB} \tag{4.3}$$

As equation 4.3 shows, in an ideal scenario with minimal noise levels, the highest SNR that can be achieved, for the signal and carrier mean optical powers considered, is 67 dB. If higher relative power levels are to be considered (for example, with higher P_s powers), P_{tot} increases, and since the minimum noise power maintains, it can be concluded that the maximum SNR achievable is even higher than 67 dB.

Figure 4.3 shows the BER as a function of the relative power level (considering $P_c = 0$ dBm), before and after SSBI removal, for different SNR values, in two different scenarios: with electrical noise considered in the SSBI estimation branch and without electrical noise considered in the SSBI estimation branch. These results were obtained without considering skew, laser phase noise and dispersion, in order to firstly assess the SSBI mitigation technique effectiveness in a more favorable scenario, where only electrical noise can be considered. Under these conditions, the SSBI estimation is not impaired by the phase noise nor by the dispersion.

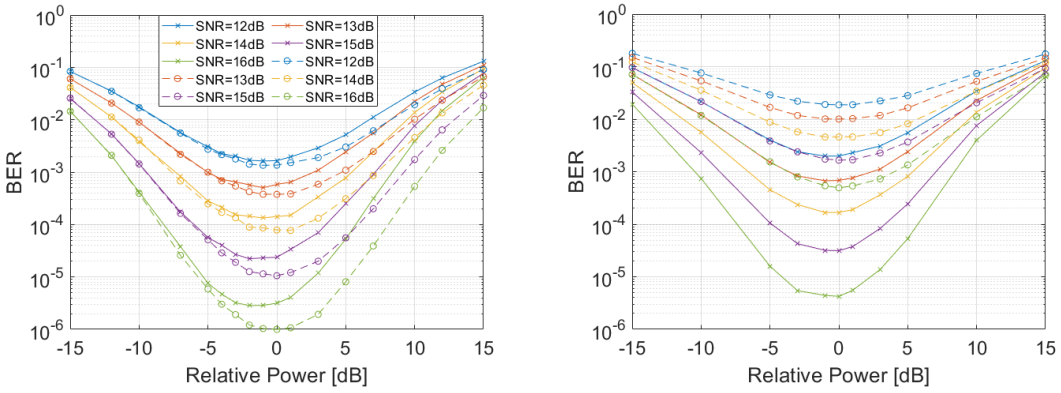

Figure 4.3: BER as a function of the relative power level before (continuous line) and after (dashed line) SSBI removal for a SNR of: 12 (blue), 13 (red), 14 (yellow), 15 (purple) and 16 (green) dB. (a) without and (b) with electrical noise in the SSBI estimation branch.

Figure 4.3 a) shows that when electrical noise is not considered in the SSBI mitigation branch, the results after SSBI mitigation starts to show beneficial to the system performance for P_r higher than -5 dB. Comparing with Figure 4.3 b), where electrical noise is considered in the SSBI estimation branch, it is noticeable that the introduced electrical noise severely corrupted the SSBI estimation and mitigation process, resulting in higher BER after removing the SSBI. This leads to the conclusion that, in presence of electrical noise, higher SNR values should be used, to avoid that the noise corrupts the SSBI mitigation. It can be seen in Figure 4.3 b) that the results before and after SSBI mitigation converge when P_r is very high. In Figure 4.4, an extension of Figure 4.3 b)

to relative power levels between 15 and 25 dB is shown. With this, system situations in which the SSBI is more powerful are tested.

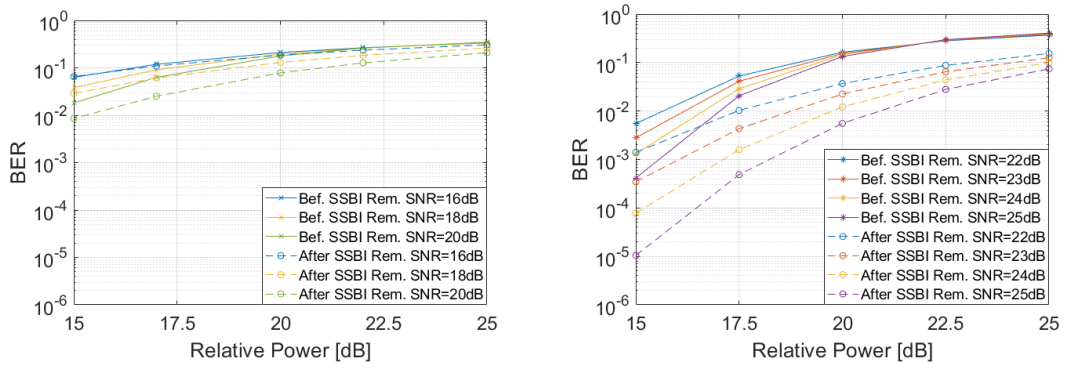

(a) (b)

Figure 4.4: BER as a function of the relative power level before (continuous line) and after (dashed line) SSBI removal, for two different sets of SNR values.

The sub-figures of Figure 4.4 consider two different sets of SNR values that were tested. When the SNR is increased, converging to a scenario of progressively less electrical noise for the same relative power level, a BER improvement is obtained after SSBI mitigation. The results indicate that the proposed scheme works whenever SSBI is dominant over other impairments. This is the case for high relative power levels (P_r) and for SNR values that guarantee a SSBI estimation not impaired by electrical noise, so that the SSBI mitigation does not come corrupted by that noise. Given that, and bearing in mind that further on it may be wanted to compensate the dispersion effect on the signal, we need to operate with such P_r and minimum SNR values, since the dispersion compensation process directly depends on a successful SSBI mitigation.

Following the results obtained in Figure 4.4, the SNR improvement due to the SSBI removal may be evaluated. This is done to demonstrate the conditions under which the system performance improvement due to SSBI mitigation is achieved. This is performed for a BER of 10^{-3} and only considering the effect of electrical noise. The required SNR improvement is defined as the difference, in dB, between the SNR needed to obtain a BER of 10^{-3} before SSBI removal and after SSBI removal. A SNR improvement of 0 dB depicts the scenario in which the same SNR value is needed to obtain a BER of 10^{-3} before and after SSBI mitigation. For this case and lower SNR improvement values, the proposed SSBI mitigation technique does not provide any advantage to the system performance.

Figure 4.5 shows the BER as a function of the SNR for different P_c and P_s with and

without SSBI mitigation. These figures are shown as examples of how the required SNR improvement study (Figure 4.6) was performed.

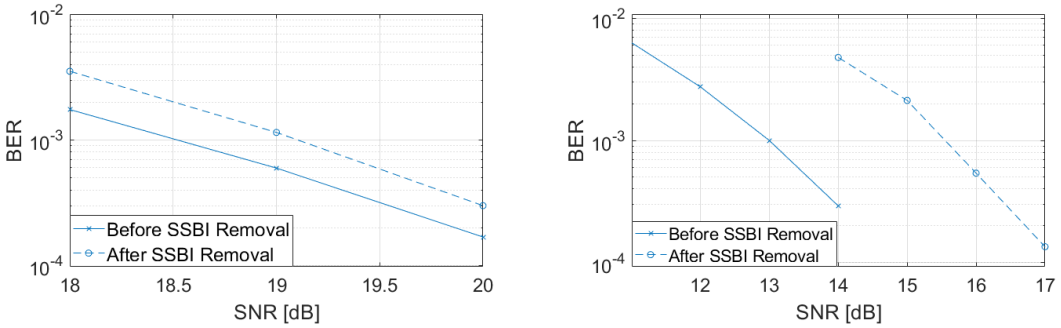

(a) P_c = -15 dBm, P_s = -4 dBm

(b) P_c = -5 dBm, P_s = -2 dBm

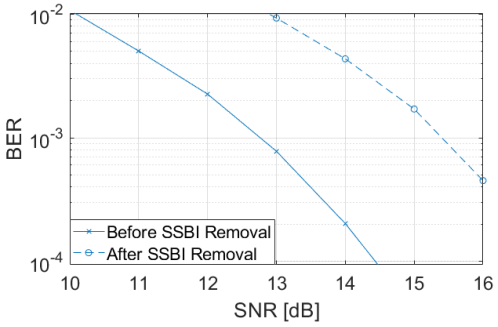

(c) P_c = 0 dBm, P_s = 2 dBm

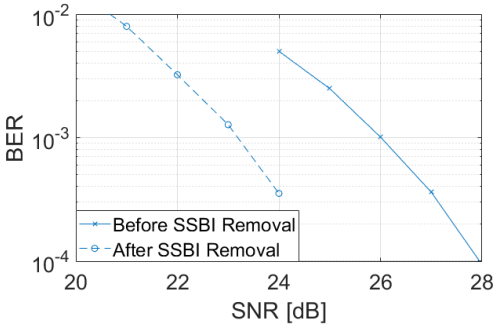

(d) P_c = 0 dBm, P_s = 16 dBm

Figure 4.5: BER as a function of the SNR for different P_c and P_s with (dashed line) and without (continuous line) SSBI mitigation.

As the results of Figure 4.5 show, if a high relative power level is not assured, the proposed SSBI mitigation technique does not show benefits, since it requires higher SNR to achieve a BER of 10^{-3}. As shown in Figures 4.5 a), b) and c), when P_s is not much higher than P_c, the system performance is worse after removing the SSBI. This occurs because under these conditions, the electrical noise is the dominant impairment (and not the SSBI), and so the SSBI estimation may be corrupted by high electrical noise levels, hence the need for higher SNR values to achieve the same BER, in comparison with the results obtained prior to SSBI removal. For example, as Figure 4.5 b) shows, a SNR of 14 dB results in a BER of 3×10^{-4} before SSBI removal, while for that same SNR, employing the proposed SSBI removal technique results in a BER of 5×10^{-3}. In the opposite way, Figure 4.5 d) demonstrates the SNR improvement obtained when P_s is much higher than P_c (16 dB higher, in this example). When the relative power level increases, the SSBI term becomes stronger, thus degrading more the system performance when SSBI mitigation is not performed. Because of this, a higher SNR is needed in order to obtain a targeted BER of 10^{-3}. In cases like the latter, employing the

proposed SSBI mitigation approach enables a SNR required improvement, achieving a BER of 10^{-3} for lower SNR values.

From the results of Figure 4.5, the SNR required to achieve a BER of 10^{-3} can be verified for P_c of -15, -10, -5 and 0 dBm and for different P_s values. Figure 4.6 shows the required SNR improvement as a function of the signal mean optical power.

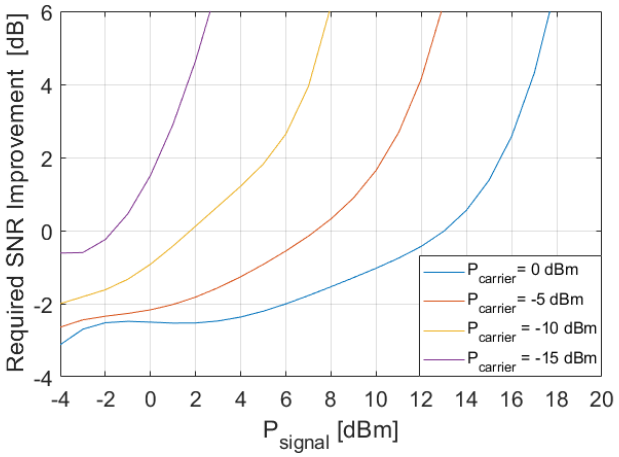

Figure 4.6: Required SNR improvement as a function of the mean optical power of the signal, for different carrier mean optical power levels.

Results in Figure 4.6 show that the SSBI removal is only effective when the mean optical power of the NRZ signal is much higher than the mean optical power of the carrier (high P_r). As an example, for a mean optical power of the carrier of -10, -5 and 0 dBm, an improvement of the SNR required when employing the SSBI removal technique to achieve a BER of 10^{-3} is obtained for P_s at least 13 dBm higher than the respective P_c. For lower signal mean optical powers, the SSBI mitigation does not show benefit to the system performance (SNR improvement required of 0 dB or less). Additionally, results of Figure 4.5 show that the key factor to obtain a given SNR improvement is the power relation (P_r) between the data signal and the carrier, and not the absolute mean optical power values of these signals. As an example, 6 dB improvement on the required SNR to achieve a BER of 10^{-3} may be accomplished with $P_c = 0$ dBm and $P_s = 18$ dBm, or with $P_c =$ -10 dBm and $P_s = 8$ dBm.

4.2 Skew impact on the system performance

In this section, the combined effect of the skew and the laser phase noise in the system performance is evaluated through BER studies. This is accomplished by comparing

the results of different laser linewidths. Each laser linewidth considered presents a different coherence time (t_c). This value can be used to assess how differently the skew affects the phase-to-intensity noise conversion. As a reference, Table 4.1 presents the coherence time of all laser linewidths under evaluation in this subsection.

Table 4.1: Coherence time for different laser linewidths.

Laser linewidth [MHz]	t_c [ns]
0.1	3183
0.5	636.6
1	318.3
5	63.66

Figure 4.7 shows the BER before and after SSBI removal as a function of the SNR with $P_r = 18$ dB, for different skew values and for the laser linewidths indicated in Table 4.1.

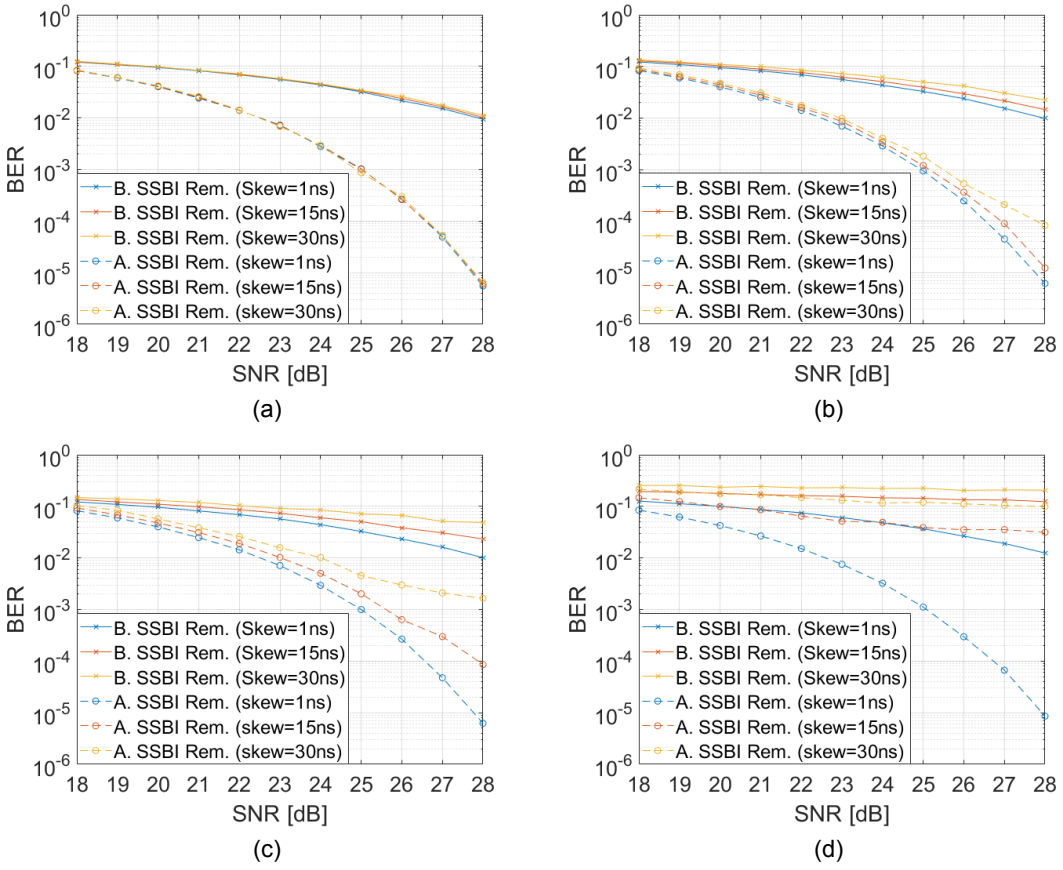

Figure 4.7: BER as a function of the SNR before (continuous line) and after (dashed line) SSBI removal considering different skew values, for $P_r = 18$ dB and a laser linewidth of: (a) 100 kHz, (b) 500 kHz, (c) 1 MHz and (d) 5 MHz.

Figure 4.7 a) shows that, for a laser linewidth of 100 kHz, the impact of the skew on the system performance is negligible. By analysing the coherence time (see Table 4.1) obtained for a 100 kHz linewidth, it can be seen that the coherence time is much higher than the skew values under test (approximately 100 times higher than 30 ns). So, the skew effect on the phase-to-intensity noise conversion is low. Figure 4.7 a) enables also to conclude that for the 100 kHz laser linewidth, a BER of 10^{-3} is reached for all skew values considered, for a SNR of 25 dB, when SSBI mitigation is employed.

When increasing the laser linewidth and thus decreasing the respective t_c, the system performance becomes more sensitive to the skew. As it can be seen in Figure 4.7 b) (linewidth of 500 kHz), the curves corresponding to the SSBI removal results start to show the effect of the laser phase noise. When increasing the skew, it can be seen that the BER starts to increase as well. Still, the coherence time corresponding to the 500 kHz linewidth is 21 times higher than the longest skew considered. So, although the effects are felt, they are not excessively degrading the system performance. For this laser linewidth, a SNR of at least 26 dB guarantees a BER lower than 10^{-3} for all skew values tested.

Figure 4.7 c) shows that the skew effect on the phase-to-intensity noise conversion starts to become significant for a linewidth of 1 MHz, degrading the system performance. For a skew of 30 ns, the coherence time corresponding to 1 MHz laser linewidth is only 10 times longer than the skew. So, it is expected (and proven by the results), that the degradation due to the phase noise severely impacts the system performance. For a skew of 30 ns, it is not possible to reach a BER lower than 10^{-3} after SSBI mitigation with SNR not exceeding 28 dB. In contrast, the laser linewidth of 1 MHz can provide a BER lower than 10^{-3} after SSBI removal, for SNR values of or above 26 dB, up to a skew of 15 ns. It is worth noting that for a skew of 15 ns, the results are identical to the results obtained for a skew of 30 ns and the 500 kHz linewidth. For both (these) cases, the relation between the skew and the laser's coherence time is the same, being the coherence time 21 times higher than the skew.

Figure 4.7 d) shows the BER results for a laser linewidth of 5 MHz. Results of Figure 4.7 d) shows that the 5 MHz linewidth has very low tolerance to the increasing skew values. With that linewidth, Figure 4.6 d) shows that the benefits of employing the proposed SSBI mitigation approach occur only for a skew of 1 ns (among the skews tested). For skew of 15 and 30 ns, the SSBI mitigation technique is not effective due to high levels of phase-to-intensity noise conversion. Bearing in mind the coherence

time corresponding to 5 MHz linewidth, and taking into account the results described throughout this subsection, it is possible to deduce that a laser with a linewidth of 5 MHz only tolerates a degradation caused by phase-to-intensity noise conversion for a maximum skew of 3 ns. In this case, the coherence time corresponding to the 5 MHz linewidth is 21 times higher than the 3 ns skew, which, as seen before, guarantees a BER under 10^{-3} for SNR values exceeding 25 dB.

In Figure 4.8, results similar to the ones shown in Figure 4.7 are presented, but for $P_r = 20$ dB. This means an increase of the difference between the NRZ signal and carrier mean optical powers.

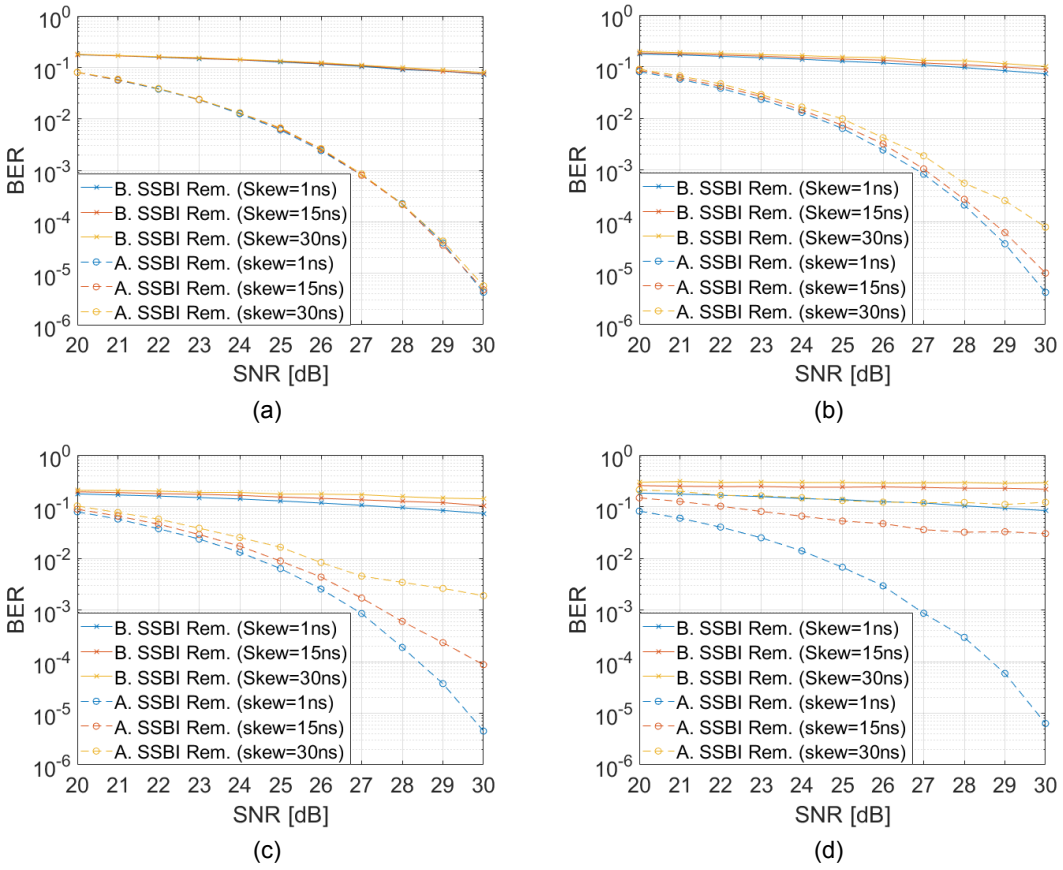

Figure 4.8: BER as a function of the SNR before (continuous line) and after (dashed line) SSBI removal considering different skew values, for $P_r = 20$ dB and a laser linewidth of: (a) 100 kHz, (b) 500 kHz, (c) 1 MHz and (d) 5 MHz.

It can be seen that the results after SSBI mitigation are similar for both P_r tested. The main difference is noted for the results before SSBI mitigation, where BER values for $P_r = 20$ dB are higher compared with the ones obtained for $P_r = 18$ dB. This occurs due to the fact that the considered NRZ signal mean optical power is even higher than the carrier mean optical power, so the SSBI term becomes stronger and more relevant.

It should be noticed that, comparing to Figure 4.7, to obtain the same results after SSBI mitigation in Figure 4.8, the range of tested SNR values goes from 20 dB to 30 dB, which shows the same increase as P_r. With this, the same noise power is considered in both scenarios, at each position of the tested SNR vector. This shows that, when removing the SSBI, the noise levels can significantly affect the effectiveness of the mitigation. If P_r increases, it means P_{tot} will be higher (for the same P_c), and the same SNR value is obtained with higher noise power (as equation 4.1 shows), meaning that the SSBI estimation is performed in presence of higher noise levels for the same SNR (comparing with Figure 4.7), which affects the SSBI removal process. As an example, for the 100 kHz laser linewidth, SNR $=$ 26 dB results in a BER not exceeding 10^{-3} for all skew values tested, when $P_r = 18$ dB, whereas for $P_r = 20$ dB the same SNR gives a BER exceeding 10^{-3} for all skew values.

To illustrate that the proposed system transmission and consequent SSBI mitigation approach is only effective in a high P_r environment and with minimum SNR values, the dependence of the BER on the SNR was assessed, for $P_r = 10$ dB and a laser linewidth of 500 kHz. The results obtained are presented in Figure 4.9. It was chosen this P_r in order to assess the system behaviour when the relative mean optical power between the signal and the carrier is not large enough.

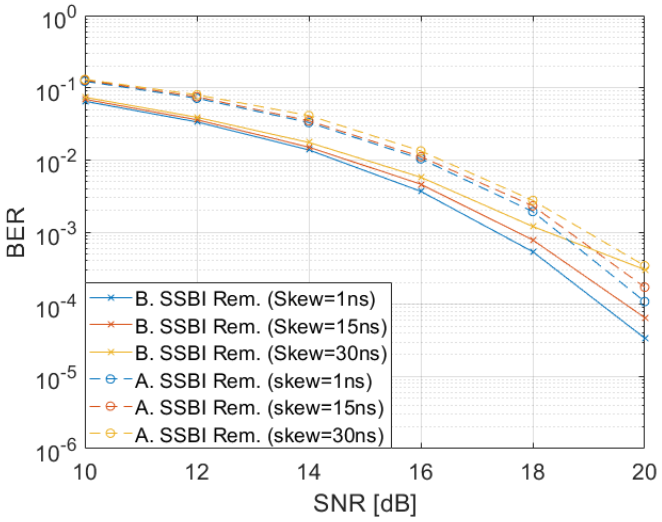

Figure 4.9: BER as a function of the SNR before (continuous line) and after (dashed line) SSBI removal considering different skew values, for $P_r = 10$ dB and a laser linewidth of 500 kHz.

The results in Figure 4.9 clearly show that, under these conditions, the SSBI removal does not show any benefit of being employed, degrading the system performance for all SNR values under test. In this scenario, the SSBI is not the dominant impairment

(P_r not high enough), and the SSBI estimation and mitigation process is corrupted by the electrical noise power. As it was aforementioned, to electronically compensate for the chromatic dispersion effects of the optical fibre at the receiver side, the SSBI needs to be effectively removed. This is not achieved under these conditions of P_r.

4.3 Dispersion impact on the system performance

In this section, the impact of the chromatic dispersion of the MCF on the system performance is quantified, in the presence of skew and laser phase noise for $P_r = 18$ dB. From the study of section 4.2, the SNR values required for a BER lower than 10^{-3} were identified. So, this study is performed for SNRs of 26, 27 and 28 dB. With lower SNR values, the BER after SSBI removal is higher than 10^{-3}, showing no interest for the scenarios under evaluation. The laser linewidths chosen for this study are 100 kHz and 5 MHz. These values are typical of external cavity lasers (ECL) and distributed feedback lasers (DFB), respectively.

Figure 4.10 demonstrates the dispersion and skew impact on the BER. Each set of curves are composed by 3 lines, which represents a SNR of 26 dB (higher BER of each set), 27 dB and 28 dB (lowest BER of each set). In order to evaluate how differently each impairment impacts the system performance, the results were obtained in the following conditions: before SSBI removal with dispersion (continuous line) and without dispersion (dashed and dotted line); after SSBI removal with dispersion (dashed line) and without dispersion (dotted line). A walk-off of 10 ns/20 km was considered. This walk-off value corresponds to one of the highest that can be found in MCFs currently [30].

Figure 4.10 a) shows the BER as a function of the MCF length for a laser linewidth of 100 kHz. Comparing with Figure 4.10 b), which shows the 5 MHz linewidth results, it is possible to conclude that very similar results are obtained. In presence of chromatic dispersion, both linewidths surpass a BER of 10^{-3} for fibre lengths longer than 180 m after SSBI removal for the most favorable case (SNR of 28 dB). In contrast, the results that emulate an ideally compensated dispersion environment (dotted and dashed and dotted lines - null total dispersion) show that the BER remains practically unchanged for the tested length. Under these conditions, the phase-to-intensity noise conversion is the only effect impacting the system performance, and the results in Figure 4.10 a)

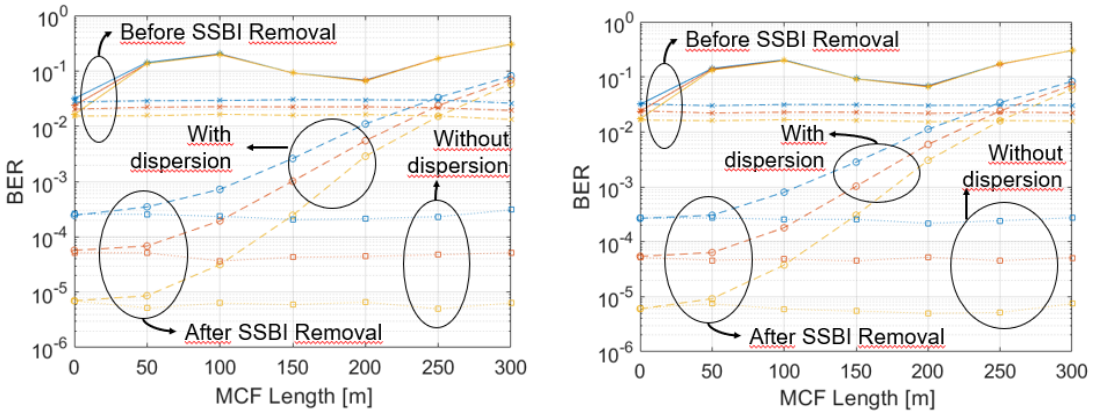

Figure 4.10: BER as a function of the MCF length, before SSBI removal with dispersion (continuous line) and without dispersion (dashed and dotted line), and after SSBI removal with dispersion (dashed line) and without dispersion (dotted line), for 10 ns/20 km walk-off and a laser linewidth of: (a) 100 kHz and (b) 5 MHz.

and b) show that, for the tested walk-off and fibre lengths, the system performance is weakly affected, regardless the analysed laser linewidth. As an example, for 300 m of MCF length, we have a skew of 0.15 ns which, as it has been shown in section 4.2, is not enough to degrade the system performance due to phase-to-intensity noise conversion.

As the results of Figure 4.10 show, for the walk-off of 10 ns/20 km, the impact of the skew and the laser phase noise on the system performance is not significant for any of the tested laser linewidths. In order to assess the tolerance of the system to the dispersion and the combined effect of the phase-to-intensity noise conversion caused by the skew, Figure 4.11 shows the BER as a function of the MCF length in similar conditions to the ones of Figure 4.10, but a very high walk-off value of 350 ns/20 km is considered. Taking into account the MCF lengths that were tested, this walk-off value was chosen in order to originate a skew that could impact the system performance due to phase-to-intensity noise conversion, jointly with the chromatic dispersion effects. With this, two separate scenarios were evaluated: one where the skew does not impact the system performance in combination with chromatic dispersion (100 kHz linewidth), and other where the skew is high enough to impact the system performance in combination with the chromatic dispersion (5 MHz linewidth).

Figure 4.11 a) shows the results for 100 kHz linewidth. For this linewidth, it can be seen that the results are similar to the results presented in Figure 4.10 a). This occurs due to the fact that, even for a very high walk-off of 350 ns/20 km, the maximum skew

obtained for the MCF lengths tested is 5 ns (for a length of 300 m). As is has been seen in the section 4.2, this skew does not cause enough degradation of the system performance due to phase-to-intensity noise conversion, for 100 kHz linewidth. On the contrary, for the 5 MHz laser linewidth (Figure 4.11 b)), the considered walk-off value clearly affects the obtained results. Comparing Figure 4.11 b) with Figure 4.10 b), it can be seen that all sets of curves highlights the impact of the combined effect of the skew and the laser phase noise (except for the curves corresponding to before SSBI removal with dispersion - which are already remarkably impaired by the SSBI and dispersion in Figure 4.10 b)). For 5 MHz laser linewidth, the results after SSBI mitigation and with dispersion are now limited to a maximum link length of approximately 125 m (for the highest SNR tested of 28 dB), opposed to the maximum link length of 180 m achieved in Figure 4.10 b). In this scenario of SSBI mitigation, even if the dispersion is fully compensated, the maximum link length is 300 m, for SNR $=$ 28 dB. For SNR $=$ 26 dB, a maximum length of 200 m is achieved, and a BER exceeding 10^{-3} occurs for longer lengths. A length of 200 m originates a skew equal to 3 ns, and this confirms that the 5 MHz laser linewidth only tolerates a skew up to 3 ns to guarantee a BER under 10^{-3} for the tested SNR values, as it has been identified in section 4.2. Nevertheless, this walk-off value is not observed in today's multi-core fibres, and the propose of this analysis of considering the walk-off of 350 ns/20 km was to identify and confirm the skew impact on different laser linewidths, and how it could, jointly with the chromatic dispersion, limit the system performance. Still, an increase of at least 100 m in the MCF length can be achieved if the SSBI mitigation approach is employed and the dispersion is totally compensated, for the tested P_r and SNR values.

4.4 Conclusions

In this chapter, the beneficial conditions under which an effective SSBI estimation and mitigation is obtained have been assessed. The impact of the combined effect of the skew and the laser phase noise on the system performance was evaluated for different laser linewidths. Then, the chromatic dispersion effect of the fibre has been considered and its impact has been quantified. The performance results have been evaluated for a maximum acceptable BER of 10^{-3}.

The results in section 4.1 show that the proposed SSBI mitigation approach only

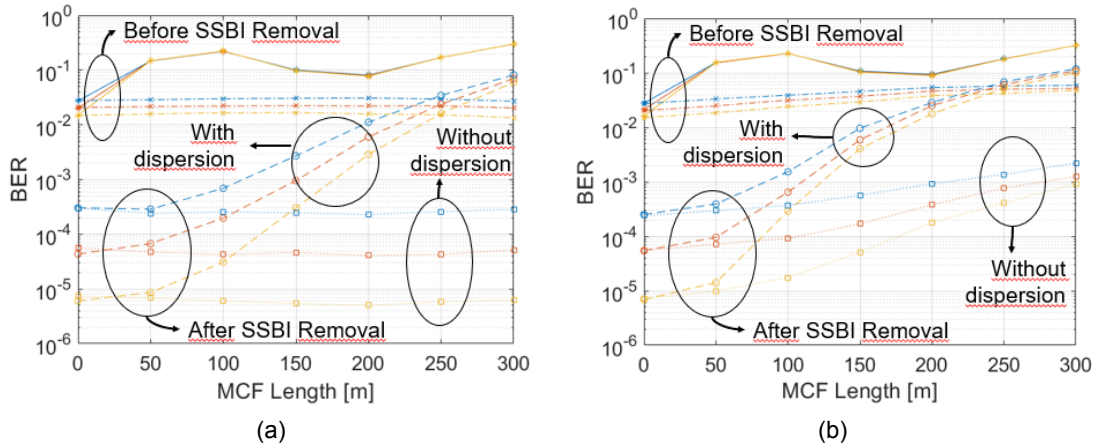

Figure 4.11: BER as a function of the MCF length, before SSBI removal with dispersion (continuous line) and without dispersion (dashed and dotted line), and after SSBI removal with dispersion (dashed line) and without dispersion (dotted line), for 350 ns/20 km walk-off and a laser linewidth of: (a) 100 kHz and (b) 5 MHz.

shows benefits of being employed with high relative power levels (P_r), where the SSBI is the dominant impairment degrading the system performance, and with SNR values that for the chosen P_r can guarantee an accurate SSBI estimation, where electrical noise does not corrupt the SSBI mitigation process. The skew impact study has shown that when the beneficial conditions for SSBI mitigation are assured, a significant performance improvement can be achieved. It has been shown that the skew impact on the phase-to-intensity noise conversion depends on the laser linewidth employed. The strength of that impact is related to the coherence time of the laser. The results show that, for SNR values exceeding 26 dB, the skew only degrades slightly the system performance when the coherence time is at least 20 times higher than the skew.

Finally, results of section 4.3 emulates a real-use MCF network, where chromatic dispersion and walk-off are inherent effects of the MCF. When chromatic dispersion compensation is not employed, the maximum link length reached is between 100 and 180 m (for the considered SNR values). This highlights the potential of using the proposed scheme for intra DC connections. Nevertheless, the higher potential of the proposed transmission scheme is achieved when dispersion compensation is electrically performed in the receiver side. This chromatic dispersion compensation is only possible after an effective SSBI mitigation. When total chromatic dispersion compensation occurs, the results show great improvement on the system performance, allowing to achieve distances higher than 300 m, possibly reaching inter DC connection lengths. However, that study is out of the scope of this work.

Chapter 5

Conclusions and future work

In this chapter, the final conclusions of the dissertation and suggestions for future work are presented.

5.1 Final conclusions

In this dissertation, a new transmission scheme for short-reach 200 Gb/s DD-based MCF optical networks, where the data signal and the virtual carrier are transmitted in separate cores of the MCF, has been proposed. Although this scheme originates a delay between the data signal and the virtual carrier due to the propagation in different cores, it enables a low-complexity SSBI mitigation approach at the receiver side to overcome the performance degradation induced by SSBI. The impact of the dispersion and the combined effect of the skew and the laser phase noise has been assessed. The system performance results presented in chapter 4 have been obtained through Monte Carlo numerical simulation.

In chapter 2, the fundamental concepts concerning this dissertation have been presented. The potential of SDM technologies, namely the MCFs, have been discussed, demonstrating how it can respond to the exponential growth of capacity demands and, at the same time, help reduce power consumption and manage space limitations on networks, particularly in intra DC systems, by enabling transmission in several cores of the same fibre cable and through multiple core equipment sharing. It has also been

shown that due to cost proposes, these short-reach networks should employ DD receivers, which are significantly impaired by SSBI.

In chapter 3, the optical system model studied in this work has been characterized and the main operation issues related to the DD-based MCF system have been evaluated, analysing in particular the impact of the phase-to-intensity noise conversion on the received NRZ signal through analysis of the corresponding eye-diagrams. The SSBI estimation technique has been introduced, showing how it can mitigate the SSBI term from the carrier-added NRZ signal after photodetection, resulting ideally in a SSBI-free signal. The laser phase noise impact on the system has been introduced and the model used in this work to emulate the laser phase noise validated, showing great correspondence between the theoretical and simulation values. The results have shown that systems employing lasers with higher linewidths are more sensitive to the skew, limiting further the system due to phase-to-intensity noise conversion. For example, a laser linewidth of 1 MHz is minimally affected by a 5 ns skew, but for a 100 ns skew the obtained eye-diagram is completely closed, reflecting a totally corrupted signal due to phase-to-intensity noise conversion. It has been shown that the laser phase noise may present significant variance in the results from transmission to transmission due to its inherent randomness, indicating that when the combined effect of the skew and the laser phase noise is severe, calculating a mean EOP should be done, in order to obtain a reliable penalty value. The results have shown that a skew of 30 ns causes a EOP of 2.8 dB for 1 MHz linewidth, whereas for 100 kHz linewidth the EOP for that same skew is 0.3 dB.

In chapter 4, it has been evaluated the system performance through BER calculations, considering firstly the combined effect of the skew and the laser phase noise and, then, also considering the chromatic dispersion effect of the fibre. It has been shown that the proposed SSBI mitigation technique is only effective when the signal mean optical power is much higher than the carrier mean optical power (high relative power level, P_r), with SNR values that lead to a SSBI estimation process not corrupted by electrical noise. For systems not impaired by dispersion, the results showed that for $P_r = 18$ dB a BER improvement (to values lower than 10^{-3}) after SSBI mitigation is obtained, for a skew of 1 ns, and for a laser linewidth up to 5 MHz, with SNR values higher than 25 dB. Also, a BER lower than 10^{-3} is achieved for a skew up to 15 ns and a maximum laser linewidth of 1 MHz, for SNR values higher than 25 dB. The results also show that increasing P_r (to 20 dB) does not show any significant difference in the after

SSBI removal results. Instead, the only difference noted is in the before SSBI results, where the system performance worsens for all studied cases due to the higher impact of the SSBI. It has been shown that the dispersion rapidly degrades the received signal quality, leading to a BER exceeding 10^{-3} for $P_r = 18$ dB and a MCF length longer than approximately 180 m, for the best tested SNR value (28 dB). When in presence of a common walk-off value (10 ns/20 km), the results show that for the considered MCF lengths, the system is not limited by the phase-to-intensity noise conversion, since the obtained results for 100 kHz laser linewidth are similar to 5 MHz laser linewidth. In this case, the originated skew is very small. Thus, the results indicate that, in absence of dispersion compensation, the proposed transmission scheme show potential to be employed in intra DC connections. However, the results suggest that in systems with full dispersion compensation, a highly significant performance improvement is achieved by the proposed SSBI mitigation technique, enabling longer connection lengths. For the tested SNR values, the results show that the maximum MCF length achieved may be much higher than 300 m.

5.2 Future work

From the work performed in this dissertation, the following proposals for future work are presented:

- Evaluate the proposed transmission scheme and SSBI mitigation technique in systems with electronic dispersion compensation;
- Investigate the implementation of the proposed transmission scheme in bidirectional connections with the objective of achieving a centralised seed carriers distribution;
- Repeat the analysis made in this work for MCF-based systems in which the transmission is realised in multiple wavelengths (WDM) and in several cores of the MCF;
- Study the impact of intercore crosstalk (ICXT) on the system performance.

5.3 Article Publication

T. Freitas, T. Alves and A. Cartaxo, “ Short-Reach 200 Gb/s SDM Network Employing Direct-Detection and Optical SSBI Mitigation”, accepted to 9º International Conference on Photonics, Optics and Laser Technology (Photoptics) in Dec. 2020, Feb. 2021.

Bibliography

[1] Cisco, “Cisco global cloud index: forecast and methodology, 2016–2021,” *White paper*, pp. 1–46, Feb. 1 2018.

[2] S. Ishimura, H. Kao, and K. Tanaka, “SSBI-free 1024QAM single-sideband direct-detection transmission using phase modulation for high-quality analog mobile fronthaul,” *IEICE Tech. Rep.*, vol. 119, no. 278, pp. 37–41, 2019.

[3] P. J. Winzer, “Spatial multiplexing: The next frontier in network capacity scaling,” *39th European Conference and Exhibition on Optical Communication (ECOC 2013)*, pp. 1–4, Sep. 2013.

[4] P. J. Winzer, D. T. Neilson, and A. R. Chraplyvy, “Fiber-optic transmission and networking: the previous 20 and the next 20 years,” *Opt. Express*, vol. 26, pp. 24190–24239, Sep 2018.

[5] D. Butler *et al.*, “Space division multiplexing in short reach optical interconnects,” *Journal of Lightwave Technology*, vol. 35, no. 4, Feb. 15 2017.

[6] C. Kachris and I. Tomkos, “A survey on optical interconnects for data centers,” *IEEE Communications Surveys & Tutorials*, vol. 14, no. 4, pp. 1021–1036, 2012.

[7] X. Zhou, R. Urata, and H. Liu, “Beyond 1 Tb/s datacenter interconnect technology: challenges and solutions,” *Optical Fiber Communications Conference and Exhibition (OFC)*, San Diego, CA, USA, Mar. 2019, paper Tu2F.5.

[8] A. Ghiasi, “Large data centers interconnect bottlenecks,” *Opt. Express*, vol. 23, pp. 2085–2090, Feb 2015.

[9] M. Glick, “Optical interconnects in next generation data centers: An end to end view,” *2008 16th IEEE Symposium on High Performance Interconnects*, pp. 178–181, Aug. 2008.

[10] Vision and Roadmap, “Routing telecom and data centers toward efficient energy use,” May. 2009.

[11] D. C. Lee, “Scaling networks in large data centers,” *2011 Optical Fiber Communication Conference and Exposition and the National Fiber Optic Engineers Conference*, pp. 1–1, March. 2011.

[12] S. Sakr, A. Liu, D. M. Batista, and M. Alomari, “A survey of large scale data management approaches in cloud environments,” *IEEE Communications Surveys Tutorials*, vol. 13, no. 3, pp. 311–336, 2011.

[13] K. Chen, C. Hu, X. Zhang, K. Zheng, Y. Chen, and A. V. Vasilakos, “Survey on routing in data centers: insights and future directions,” *IEEE Network*, vol. 25, pp. 6–10, July 2011.

[14] J. Perin, A. Shastri, and J. Kahn, “Data center links beyond 100 Gbit/s per wavelength,” *Optical Fiber Technology*, vol. 44, pp. 69–85, 2018.

[15] T. Hayashi, T. Nagashima, T. Morishima, Y. Saito, and T. Nakanishi, “Multi-core fibers for data center applications,” pp. 1–4, 2019.

[16] D. J. Richardson, J. M. Fini, and L. E. Nelson, “Space-division multiplexing in optical fibres,” vol. 7, p. 354–362, Apr 2013.

[17] W. Klaus *et al.*, “Advanced space division multiplexing technologies for optical networks,” *Journal of Lightwave Technology*, vol. 9, no. 4, pp. 1–11, Apr. 4 2017.

[18] J. Sakaguchi, B. J. Puttnam, W. Klaus, Y. Awaji, N. Wada, A. Kanno, T. Kawanishi, K. Imamura, H. Inaba, K. Mukasa, R. Sugizaki, T. Kobayashi, and M. Watanabe, “19-core fiber transmission of 19x100x172-Gb/s SDM-WDM-PDM-QPSK signals at 305 Tb/s,” *OFC/NFOEC*, pp. 1–3, March 2012.

[19] H. Takara, A. Sano, T. Kobayashi, H. Kubota, H. Kawakami, A. Matsuura, Y. Miyamoto, Y. Abe, H. Ono, K. Shikama, Y. Goto, K. Tsujikawa, Y. Sasaki,

I. Ishida, K. Takenaga, S. Matsuo, K. Saitoh, M. Koshiba, and T. Morioka, “1.01-Pb/s (12 SDM/222 WDM/456 Gb/s) crosstalk-managed transmission with 91.4-b/s/Hz aggregate spectral efficiency,” *European Conference and Exhibition on Optical Communication*, 2012.

[20] K. Saitoh and S. Matsuo, “Multicore fiber technology,” *Journal of Lightwave Technology*, vol. 34, no. 1, pp. 55–66, Jan. 1 2016.

[21] A. M. Ortiz and R. L. Sáez, “Multi-core optical fibers: Theory, applications and opportunities,” *Selected Topics on Optical Fiber Technologies and Applications*, 2018.

[22] T. Hayashi and T. Nakanishi, “Multi-core optical fibers for the next-generation communications,” *SEI Technical Review,* no. 86, pp. 23–28, Apr. 2018.

[23] T. M. F. Alves and A. V. T. Cartaxo, “Characterization of the stochastic time evolution of short-term average intercore crosstalk in multicore fibers with multiple interfering cores,” *Opt. Express*, vol. 26, pp. 4605–4620, Feb 2018.

[24] T. Alves and A. Cartaxo, “Decorrelation bandwidth of intercore crosstalk in weakly coupled multicore fibers with multiple interfering cores,” *Journal of Lightwave Technology*, vol. 37, no. 3, pp. 744–754, Feb. 1 2019.

[25] T. Hayashi, T. Taru, O. Shimakawa, T. Sasaki, and E. Sasaoka, “Characterization of crosstalk in ultra-low-crosstalk multi-core fiber,” *Journal of Lightwave Technology*, vol. 30, pp. 583–589, Feb 2012.

[26] T. Alves and A. Cartaxo, “Intercore crosstalk in homogeneous multicore fibers: theoretical characterization of stochastic time evolution,” *Journal of Lightwave Technology*, vol. 35, no. 21, p. 4613–4623, Nov. 1 2017.

[27] B. J. Puttnam, R. S. Luís, E. Agrell, G. Rademacher, J. Sakaguchi, W. Klaus, G. M. Saridis, Y. Awaji, and N. Wada, “High capacity transmission systems using homogeneous multi-core fibers,” *Journal of Lightwave Technology*, vol. 35, March 2017.

[28] T. Alves, J. Rebola, and A. Cartaxo, “Outage probability due to intercore crosstalk in weakly-coupled MCF systems with OOK signaling,” *Optical Fiber Communications Conference and Exhibition (OFC)*, San Diego, CA, USA, Mar. 2019, paper M2I.1.

[29] A. Udalcovs, R. Lin, O. Ozolins, L. Gan, L. Zhang, X. Pang, R. Schatz, A. Djupsjöbacka, M. Tang, S. Fu, D. Liu, W. Tong, S. Popov, G. Jacobsen, and J. Chen, "Inter-core crosstalk in multicore fibers: Impact on $56-$ Gbaud$/\lambda$ /core PAM-4 transmission," in *2018 European Conference on Optical Communication (ECOC)*, pp. 1–3, 2018.

[30] G. Rademacher, R. Luís, B. Puttnam, Y. Awaji, and N. Wada, "Crosstalk dynamics in multi-core fibers," *Optics Express*, vol. 25, no. 10, May. 15 2017.

[31] T. M. F. Alves, L. M. M. Mendes, and A. V. T. Cartaxo, "High granularity multiband ofdm virtual carrier-assisted direct-detection metro networks," *Journal of Lightwave Technology*, vol. 33, pp. 42–54, Jan 2015.

[32] J. C. Cartledge and A. S. Karar, "100 Gb/s intensity modulation and direct detection," *J. Lightwave Technol.*, vol. 32, pp. 2809–2814, Aug 2014.

[33] K. Zhong, Wei Chen, Qi Sui, J. Man, Alan Pak Tao Lau, Chao Lu, and Li Zeng, "Experimental demonstration of 500 Gbit/s short reach transmission employing PAM4 signal and direct detection with 25 Gbps device," *2015 Optical Fiber Communications Conference and Exhibition (OFC)*, pp. 1–3, March 2015.

[34] N. Eiselt, H. Griesser, J. Wei, A. Dochhan, M. Eiselt, J. Elbers, J. J. V. Olmos, and I. T. Monroy, "Real-time evaluation of 26-GBaud PAM-4 intensity modulation and direct detection systems for data-center interconnects," *2016 Optical Fiber Communications Conference and Exhibition (OFC)*, pp. 1–3, March 2016.

[35] S. Kanazawa, H. Yamazaki, Y. Nakanishi, T. Fujisawa, K. Takahata, Y. Ueda, W. Kobayashi, Y. Muramoto, H. Ishii, and H. Sanjoh, "Transmission of 214-Gbit/s 4-PAM signal using an ultra-broadband lumped-electrode EADFB laser module," *Optical Fiber Communication Conference Postdeadline Papers*, pp. 1–3, March 2016.

[36] X. Chen, C. Antonelli, S. Chandrasekhar, G. Raybon, J. Sinsky, A. Mecozzi, M. Shtaif, and P. Winzer, "218-Gb/s single-wavelength, single-polarization, single-photodiode transmission over 125-km of standard singlemode fiber using Kramers-Kronig detection," *2017 Optical Fiber Communications Conference and Exhibition (OFC)*, pp. 1–3, March 2017.

[37] M. Chagnon, S. Lessard, and D. V. Plant, "336 Gb/s in direct detection below KP4 FEC threshold for intra data center applications," *IEEE Photonics Technology Letters*, vol. 28, pp. 2233–2236, Oct 2016.

[38] M. Morsy-Osman, M. Chagnon, M. Poulin, S. Lessard, and D. V. Plant, "224-Gb/s 10-km transmission of PDM PAM-4 at 1.3 μm using a single intensity-modulated laser and a direct-detection MIMO DSP-based receiver," *Journal of Lightwave Technology*, vol. 33, pp. 1417–1424, April 2015.

[39] W. Lv, J. Li, and K. Xu, "Direct detection of PAM4 signals with receiver-side digital signal processing for bandwidth-efficient short-reach optical transmissions," *2016 IEEE Optoelectronics Global Conference (OGC)*, pp. 1–3, Sep. 2016.

[40] S. T. Le, K. Schuh, M. Chagnon, F. Buchali, R. Dischler, V. Aref, H. Buelow, and K. M. Engenhardt, "1.72-Tb/s virtual-carrier-assisted direct-detection transmission over 200 km," *Journal of Lightwave Technology*, vol. 36, pp. 1347–1353, March 2018.

[41] Shi, Yuan, C.-H. Huang, L. Yun, Lu, Y.-F. Luo, and Yue, "Bias controller of Mach–Zehnder modulator for electro-optic analog-to-digital converter," *Micromachines*, vol. 10, p. 800, November 2019.

[42] L. N. Binh, *Optical fiber communication systems with Matlab and Simulink models; 2nd Edition.* Optics and photonics (CRC Press), Hoboken, NJ: CRC Press, 2014.

[43] *Recommendation ITU-T G.652: Characteristics of a single-mode optical fibre and cable*, International Telecommunication Union, Telecommunication Standardization Sector, 2016.

[44] G. Agrawal, *Fiber-Optic Communication Systems*. John Wiley & Sons, 4^{th} ed., 2010.

[45] A. Cartaxo and T. Alves, *Laboratório de Comunicações Ópticas*. Departamento de Ciências e Tecnologias da Informação, ISCTE-Instituto Universitário de Lisboa, 2019.

[46] X. Xie, R. Bouchand, D. Nicolodi, M. Lours, C. Alexandre, and Y. L. Coq, "Phase noise characterization of sub-hertz linewidth lasers via digital cross correlation," *Opt. Lett.*, vol. 42, pp. 1217–1220, Apr 2017.

[47] K. Ho, *Phase-Modulated Optical Communication Systems*. Springer US, 2005.

[48] W. Peng, “Analysis of laser phase noise effect in direct-detection optical OFDM transmission,” *Journal of Lightwave Technology*, vol. 28, no. 17, pp. 2526–2536, 2010.

[49] G. Einarsson and M. Leeson, *Principles of Lightwave Communications*. Wiley, 1996.

[50] J. Goodman, *Statistical Optics*. Wiley Series in Pure and Applied Optics, Wiley, 2015.

Appendix A

Electrical noise model

When considering PIN photodetectors, one of its main disadvantages is that it is limited by the circuit noise. The circuit noise (thermal noise) generated by the load resistor, R_L, can be modeled by a zero mean Gaussian distribution with the variance of the current noise given by [45]

$$\sigma_c^2 = \frac{4k_B T_K}{R_L} \cdot f_{n,e}\, B_{e,n} \tag{A.1}$$

where k_B = 1.38 x 10^{-23} J/K is the Boltzmann constant, T_K = 290 K is the room temperature in Kelvin, $f_{n,e}$ = 6 dB is the noise figure and $B_{e,n}$ is the noise equivalent bandwidth of the electrical filter of the optical receiver given by

$$B_{e,n} = \int_0^{+\infty} \left| \frac{H(f)}{H(0)} \right|^2 df \tag{A.2}$$

where $H(f)$ is the frequency response of the electrical filter. However, to generate the Gaussian noise in simulation it cannot be used the circuit noise equation represented above (equation A.1). Instead, it has to be used the two-sided PSD of the current noise given by [45]

$$S_c = \frac{\sigma_c^2}{B_{e,n}} \cdot \frac{1}{2} = \frac{2k_B T}{R_L} \cdot f_{n,e} \quad \left[\mathrm{A}^2/\sqrt{\mathrm{Hz}}\right] \tag{A.3}$$

where $\frac{1}{2}$ factor is used to obtain the two-sided equation of the PSD. Then, the noise power, P_n, is obtained as follows

$$P_n = \int S_n\, df = S_c \cdot f_s \tag{A.4}$$

where f_s represents the sampling frequency. With this, the noise power is calculated in the simulator and added to the output of the PIN, in order to accurately simulate the electrical noise generated in the photodetection process.

Appendix B

Bit error rate

In this work, the figure of merit used to assess the system performance is the BER, where the performance of the optical transmission system is evaluated from the occurrence of errors in the received bits. There are different ways of estimating the BER: through a semi-analytical or fully analytical approach, or by direct-error counting (DEC). The DEC approach is the performance measure used in the BER calculations presented in Chapter 4.

The DEC provides excellent BER accuracy, although requiring that the transmitted bits are large, which can sometimes lead to very long computation times. To perform the DEC, a Monte Carlo simulation is implemented, where sampled values of the input bit sequence and noise samples are generated, then the samples are processed through the models of the functional blocks that emulates the communication system, and finally the output is analysed, estimating the BER value as follows [45]:

$$P_b = \frac{1}{N} \sum_{k=1}^{N} z[k] \tag{B.1}$$

where *N* represents the sample values of the input bit sequence, and $z[k]$ equals to 0 or 1, if the output bit sample corresponds to the input bit or not (error), respectively. This decision to determine if it is an error or not is made by a threshold level. If the bit sample is higher than the threshold, it corresponds to a bit 1. If it is lower corresponds to a bit 0. After doing this, it is possible to compare the output sequence with the input sequence and compare bit by bit to discover the number of errors and estimating the BER as shown in equation B.1.

In order to present reliable BER results, it is important to verify the fluctuation obtained in the BER caused by the inherent randomness associated with the phase-to-intensity noise conversion. Figure B.1 presents a study done to obtain the average BER after SSBI removal as a function of the number of runs. Each run represents a simulation cycle where at least 100 errors or more were reached (calculated as shown in equation B.1). Different samples of the laser phase noise process are generated in each run. Then, the average BER is calculated by computing the mean BER of all BER values obtained to that point (number of runs performed). These results were taken for a P_r of 18 dB, a laser linewidth of 1 MHz, a skew of 30 ns and SNR of 28 dB. Under these conditions, the impact of the combined effect of the skew and the laser phase noise is significant, which may cause high fluctuation in the number of errors. Still, the conditions chosen for this study guarantee that the received signal is not fully impaired by the SSBI, since in those cases the BER does not show great variance given that it is always very high due to the great amount of errors encountered.

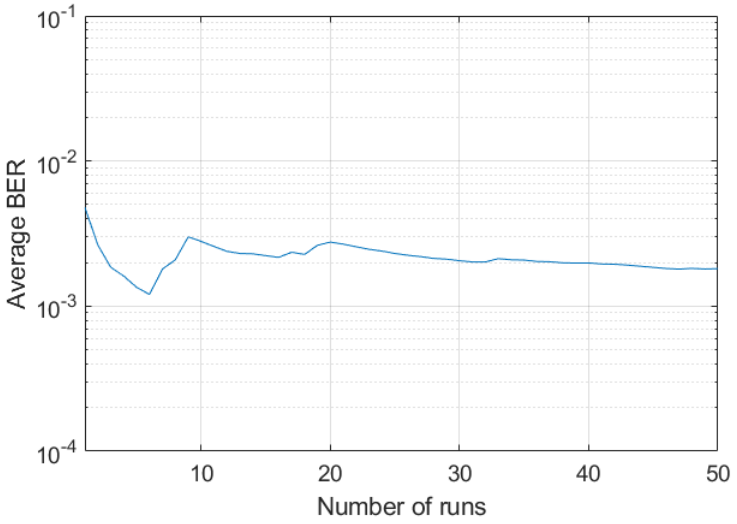

Figure B.1: Average BER as a function of the number of runs.

Figure B.1 shows that the BER fluctuation starts to soften around 30 runs. For this reason, all BER values calculated in a situation where the laser phase noise significantly impacts the final results (predictable comparing the skew and the t_c of the laser linewidth) are obtained by averaging the BER over 30 runs, so that the results presented reflect a situation where the BER obtained is always stabilised. For low skew values (as 1 ns, frequently used in the simulations), because it has minimal or no impact on the system performance and the obtained BER can be too low (causing long computational times), between 1 and 3 runs are considered to get the final BER.